Engineering Structures 296 (2023) 116967

Contents lists available at ScienceDirect

Engineering Structures

journal homepage: www.elsevier.com/locate/engstruct

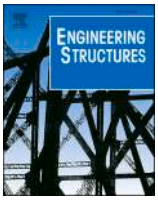

Full-scale cyclic tests on a stone masonry building to investigate the effectiveness of a one-side application of the composite reinforced mortar system

Natalino Gattesco [a], Emanuele Rizzi [a,*], Ingrid Boem [a], Luca Facconi [b], Fausto Minelli [b], Allen Dudine [c], Matija Gams [d]

[a] University of Trieste, Department of Engineering and Architecture, Via Alfonso Valerio 6/1, 34127 Trieste, Italy
[b] University of Brescia, Department of Civil, Environmental, Architectural Engineering and Mathematics, via Branze 43, 25123 Brescia, Italy
[c] Fibre Net S.p.a., Via Jacopo Stellini, 3 – Z.I.U., 33050 Pavia di Udine (UD), Italy
[d] University of Ljubljana, Faculty of Civil and Geodetic Engineering, Jamova 2, 1000 Ljubljana, Slovenija

ARTICLE INFO

Keywords:
Composites
Glass fiber
Structural rehabilitation
Masonry structures
Earthquake engineering
Full-scale experimental test

ABSTRACT

The results of an experimental study on a full-scale, two-storey rubble stone masonry building, strengthened with a Composite Reinforced Mortar (CRM) system applied on the external face of the walls, are herein presented. The CRM system consisted of a mortar coating reinforced with Glass Fiber Reinforced Polymer (GFRP) mesh and injected steel transverse connectors, which connect the separated wythes of the masonry. The aim of the research is to investigate the effectiveness of this strengthening technique. The study concerns two cyclic experimental tests: the first was carried out on the unreinforced masonry building up to a damage level not far from the ultimate limit state. Then, the building was repaired, strengthened with the proposed technique, and tested again. The second test was carried out up to a near-collapse condition. This allowed to evaluate the effectiveness in terms of seismic performances provided by the reinforcement.

The cyclic horizontal load, with increasing amplitude, was applied to each of the two longitudinal walls of the building by means of servo-controlled hydraulic jacks pinned to a vertical steel beam. This beam allowed the distribution of the total lateral force between the first floor and roof level, in the fundamental mode shape. The experiments proved the effectiveness of the proposed strengthening method: with respect to the unreinforced masonry building, the resistance increased by 2.4 times, the displacement capacity by 4 times and the total dissipated energy by about 7.2 times. These benefits were due to the GFRP mesh reinforced coating's capability to prevent the formation of isolated thick cracks, instead promoting a wider dispersion of many closely spaced thin cracks. Moreover, the importance of transverse connectors in preventing the separation of the masonry leaves in the strengthened walls was also clearly observed.

1. Introduction

Masonry is one of the most used construction materials for residential buildings in different European regions and countries worldwide. In particular, unreinforced stone masonry represents the common building material for traditional residential constructions of hilly and mountain areas. Most of the existing masonry constructions built in the last centuries have a maximum of three storeys, with floors made mainly with timber joists and perpendicular boards or with wrought iron beams and shallow masonry vaults. As they were mostly designed before the introduction of seismic provisions in structural codes, these buildings typically present a high seismic vulnerability. In fact, the low in-plane stiffness of the floors and the mere support of the beams on the bearing walls do not allow the building to have a box-like behaviour, which would grant the structures a significant resistance and ductility increase when subjected to earthquakes. In addition, the lack of a proper connection between orthogonal walls could cause out-of-plane collapses. It is also very common to observe the presence of multi-leaf bearing walls, sometimes with an inner cavity filled with scrap material and low-strength mortar. When subjected to horizontal loads, the

* Corresponding author.
E-mail address: emanuele.rizzi@units.it (E. Rizzi).

https://doi.org/10.1016/j.engstruct.2023.116967
Received 19 April 2023; Received in revised form 24 August 2023; Accepted 24 September 2023
Available online 29 September 2023

heterogeneity of materials, the low tensile and shear strength, and the possible separations of leaves arise as significant vulnerability factors. Further potential threats may also be related to the building configuration, like the presence of extended gable walls, arches/vaults, and untied inclined roofs, which increase the horizontal loads supported by the bearing walls.

Current engineering knowledge enables the assessment of the importance of seismic retrofitting historical structures. The need to find an efficient and economical way to improve the structural response of these buildings has led to the development of various strengthening techniques. Among all, fibre-reinforced coatings, have attracted increasing attention and have been investigated in several studies [1]. Basically, the effectiveness of these techniques results from the high tensile strength of the fibers embedded in the coating, which increases the shear and bending capabilities of the masonry walls in terms of strength and displacement capacity. The first experiences and investigations focused on the application on both wall sides, which was structurally balanced and enabled large improvements in seismic performance. Since then, the research has progressively gained a deep understanding of the CRM systems and their interaction with the masonry. Single-sided applications are increasingly attracting the interest of the market and researchers for several reasons. The construction is faster and cheaper, the activities inside the building are not interrupted during construction, and the occupants don't need to find alternate accommodations. Furthermore, valuable artistic decorations can be preserved on the inside (or outside, when the inside side application is preferred). On the other hand, even though cheaper, faster and more practical, the application of the fibre-reinforced coatings just on one side limits the amount by which bearing walls can be strengthened and, thus, the attainable seismic performance improvement. Therefore, the choice between single- or double-sided application should be made according to the current building performances and the seismic demand. Moreover, the effectiveness of one-side application in multi-leaf masonry could be limited by premature leaves separation, especially in the case of frequent load reversals (typical in seismic events) combined with large axial stresses [2]. The use of properly designed transverse connectors has proved effectiveness in preventing or significantly delaying such an occurrence [3,4,5,6].

The broad literature reviews recently carried out by Boem [7,8] gathered numerous and wide-ranging experimental results related both to the mechanical and chemical behaviour of the fiber-based mortar compounds and to the testing of masonry strengthened by using such techniques. On the latter subject, it emerged that most of the effort was devoted to testing simple, isolated piers and spandrels subjected to elementary in-plane or out-of-plane actions. But testing entire structures is a fundamental step to check the effectiveness of the reinforcement at the global level, under the actual interactions among the resisting elements and actual boundary conditions; it also provides useful outputs for the validation of procedures and tools aimed at the global performance analysis. Nevertheless, as a consequence of the high costs and great complexity, full-scale tests on strengthened structures are currently rare.

The seismic load on the structure was simulated by applying horizontal forces to the different floors, gradually increasing the amplitude of the deformation cycles (quasi-static cyclic tests). Gu et al. [9] tested a 1/3-scale, three-storey, solid brick masonry wall with openings under in-plane quasi-static cyclic loading. In this study the strength and size of the bricks and the mortar were not scaled accordingly due to challenges in determining compatible scale factors among structures and materials. They compared the behaviour before and after the repair by carbon FRP grids bonded with epoxy resin on one side and only at the areas of intensive cracking on the ground floor. Under an area-based reinforcement ratio of 18 %, the walls' lateral resistance was restored to 82 % of the undamaged wall, and ductility and energy dissipation capacity were effectively recovered or enhanced.

Triller et al. [10] performed quasi-static cyclic tests on a full-scale three-storey hollow-bricks masonry building, comparing the seismic response before and after the retrofitting with a double-side application of mortar coating reinforced with glass fiber grids. Glass fiber anchors were used to provide inter-storey connection and anchoring into the foundation. The building resistance increased by approximately 50 %, and the deformation capacity and ductility tripled. It was also clearly pointed out the important role of adequate confining (wrapping) and anchoring the coating to the existing masonry.

The study made by Lucchini et al. [11] investigated, through full-scale quasi-static cyclic tests on a two-storey hollow-block masonry building, the effectiveness of the one-side application of a 30 mm thick mortar coating added with short steel fibers (i.e., Fiber Reinforced Mortar), combined with conventional steel reinforcing bars located at the base of the building to provide a connection with the foundation. In addition, steel connectors (about 6 connectors per square meter) were also installed to link the coating layer to the masonry walls. The strengthened configuration highlighted a significant increase of the lateral initial stiffness and resistance capacity (2.3 and 3.3 times higher, respectively), and ensured an effective ultimate drift of up to 0.4 %.

Morici et al. [12] performed on-site pushover tests on two almost identical two-storey brick masonry buildings previously damaged by a seismic event. One was repaired by repointing the cracks, and the other was strengthened with a CRM coating reinforced by glass fiber-reinforced polymer meshes, applied on both sides of the load-bearing walls of the first level and only on the outer face at the second level. Horizontal steel tie-rods were also introduced on the intermediate floor and roof. Both structures were subjected to a monotonic, quasi-static lateral load. According to the test results, the second structure exhibited a resistance and top displacement capacity, which were respectively 2.8 and 1.8 times higher than those presented by the first one. It is worth remarking that the CRM benefits were not fully exploited because of some uplift at the base of the building, which clearly pointed out the importance of an effective connection of the coating at the foundations.

More complex than quasi-static loading tests is the shaking table test, in which the structure is subjected to a series of dynamic actions (simulating the earthquake ground motions) of increasing intensity.

Maddaloni et al. [13] studied the dynamic behaviour of a 1:2 scaled, single-storey simple building made of regular tuff masonry and covered by a flat timber floor with a cementitious deck. The as-built structure was damaged, repaired by means of cracks injection and stitching, and then externally retrofitted with a diffuse fiber-reinforced plastering of the facades combined with the top wrapping by glass fibre grids embedded in the mortar coating. The intervention prevented the activation of local failures, restored the original frequency and improved the building's resistance to a +40 % input acceleration without any significant damage. The specimen behaved as a monolithic block with a rigid rotation at the base because it was not anchored into the foundation.

De Santis and de Felice [14] performed shaking table tests on a full-scale, tuff masonry room with openings covered by an inclined timber roof. The sample was tested both unstrengthened and after retrofitting with CRM applied on the outer surface of the two walls with openings. As compared to the unstrengthened specimen, the absolute base acceleration attained by the retrofitted structure under ultimate conditions was more than doubled, and the collapse moved from wall separation to in-plane mechanism. After adding a horizontal top steel tie bar on the unstrengthened wall, the acceleration resulted four times higher.

Juhásová et al. [15] carried out dynamic investigations on a single-level stone masonry room. At first, the configuration reinforced by means of polymer grids embedded in some bed joints was tested. Then, the structure was retrofitted by means of polymer grids bonded on the outer surface with a fibre-reinforced plaster. The maximum input acceleration of the repaired model was more than tripled; the damage pattern revealed an effective inhibition of the out-of-plane mechanism of the walls, in favour of a box-like behaviour, with most of the damage accumulated at the base (due to the lack of a plaster connection with the foundations).

Referring to strengthening methods other than fiber-based, it is

worth mentioning the research work of Benedetti et al. [16], that tested on a shaking table a total of 24, half scaled, two-storey masonry buildings, made either of solid brick and stone masonry. The study compared the effectiveness of different traditional retrofitting techniques such as steel ties, steel beams and reinforced concrete bands, in preventing walls separation and improving the connection between slabs and walls. Similarly, Mazzon et al. [17] compared the dynamic tests results of two identical stone masonry houses, 2:3 scaled, and highlighted the capability of hydraulic lime grout injections to substantially increase the resistant capacity (+56 % maximum input acceleration) without modifying the original frequency and modal deformations.

It is also significant to mention the shaking-table tests of Magenes et al. [18,19] and Senaldi et al. [20], which was carried out to investigate on the effects of traditional seismic retrofitting techniques aimed at fostering the box-type global behaviour of the structure. The samples consisted of three full-scale, two-storey, double-leaf stone masonry buildings with flexible timber floors and roofs (single layer of planks). The 1st prototype [18] represented a vulnerable building without anti-seismic detailing and devices: the introduction, in the damaged configuration, of perimeter tie-rods at the floor and roof level and cable bracings under the roof, and the improvement of the connection of the ridge beam with the gable walls, let the structure to withstand an 18 % greater maximum acceleration. In the 2nd prototype building [19], an additional layer of matchboard planks was applied to provide moderate in-plane stiffening of the wooden diaphragms, and the wall-to-diaphragm connections were improved by introducing steel ring beams on the intermediate floor, and reinforced masonry ring beams, at the top. Differently, the 3rd prototype building [20] had the roof diaphragm stiffened by multilayer plywood panels connected to perimeter reinforced concrete beams. The intermediate floor was stiffened by a reinforced concrete slab provided with embedded bars for connection with the masonry. The buildings 2 and 3 were able to withstand, respectively, accelerations up to 1.84 and 2.37 times higher than the reference configuration.

In Vintzileou et al. [21], the shaking table tests of a 1/2 scaled, two-storey building showed that the stiffening of the wooden floors by means of an additional plank layer, combined with grout injections on the masonry infill walls, led to the doubling of the resisting accelerations. Similarly, Guerrini et al [22], tested a 1/2 scaled, three-storey, stone masonry aggregate composed of two units on a unidirectional shaking table, and obtained an 83 % acceleration increase by installing floor tie rods and improving the wall-to-diaphragm assembly by means of steel devices connecting the floor joists with the outer wall face.

The experimental tests presented in this paper concerned full-scale cyclic tests on a two-leaf rubble stone masonry building. The tests were recently carried out at the Laboratory of the University of Brescia (Italy) as part of the Interreg Italia-Slovenija Project "CONSTRAIN" [23]. The project studied innovative strategies for the seismic protection of existing masonry buildings, by the targeted use of modern fiber-reinforced composite materials for strengthening top beams, floor ties and reinforced plasters to be applied outside of the buildings. For such a purpose, a full-scale masonry building and other masonry samples (piers, spandrels, C-walls, top beams) were designed, built, and tested in order to optimize the materials as well as the coating application technique and to assess the effectiveness of the strengthening intervention. An overview of the testing campaign is reported in Gattesco et al. [24]. The retrofitting approach investigated in this study is primarily intended to be used for buildings that require interventions while maintaining internal activities (external intervention).

The full-scale structure was designed to represent a historical rural stone masonry house typical of the Italian and Slovenian heritage [25]. In fact, in those countries, simple two/three-story rectangular buildings provided with wood-joist floors and a pitched timber roof covered by tiles are very common. The bearing walls are generally made of roughly sized stones and a modest amount of low strength lime mortar. The test was subdivided into two stages (test on the unstrengthened and on the retrofitted structure) to simulate a repairing intervention on a building that was pre-damaged by a significant seismic event. The intervention technique consisted of a CRM system applied on the building facades, with the addition of transverse injected steel connectors to increase the collaboration between the masonry wall leaves, steel tie rods at the first floor and on the roof rafters. The structure was continuously monitored during the tests by using load cells, displacement transducers and a digital image correlation (DIC) system. The natural periods of vibration of the structure were also identified to examine the stiffness degradation after damage and the variations due to strengthening.

In the following, the main characteristic of the building, the strengthening intervention, and of the tests' arrangements are described in detail. Then, the results of the tests are reported, broadly analyzed, and discussed, including data and considerations on the effectiveness of the retrofitting technique, on dissipated energy and on damping factors.

2. Building characteristics

The two-storey building consisted of four unreinforced masonry bearing walls (i.e., North, West, South, and East wall – Fig. 1), a wooden intermediate floor (Fig. 2a) and a gabled timber roof (Fig. 2a). The structure had in-plane dimensions 5750x4350 mm, with a total height at rooftop of 6733 mm. The main geometric characteristics are schematically shown in Fig. 3. Each pier was identified by a label indicating the wall orientation (*N*, *S*, *W*, *E*), followed by letter "*p*" for piers, the indication of the building level (1 or 2) and a sequential latter (*a*, *b*, *c*). The aspect ratio (height to width) of the longitudinal piers of the base floor ranged from 1.1 to 2.0.

The 350 mm thick bearing walls were made of sandstone units with approximate dimensions of 150 × 100 × 210 mm (width × height × length), laid in a two-leaf masonry configuration (Fig. 4). The stones forming the two leaves of the wall were laid so to obtain continuous bed joints. Due to the rough size of the stones, several efforts were made to select and cut them to ensure discontinuity in vertical joints and equal thickness of the wall leaves. As it occurs in actual buildings, the two leaves were not connected by transversal stones (headers) crossing the whole wall thickness. Both head and bed joints had an average thickness of 10 mm and were filled with a pre-mixed lime-based mortar. The stone masonry was built with a mix of two different Credaro stones, respectively named Berrettino and Medolo, which have approximate compressive strengths of 170 MPa and 150 MPa, respectively. These stones belong to the sandstone type with a calcareous composition. Berrettino is a rock made of minute detrital grains, mainly carbonate (calcarenite), with evident stratification levels, and it is yellow–brown or pink. In contrast, Medolo is a rock almost entirely made of microcrystalline calcium carbonate (crystalline limestone) with a very fine grain size, and it is hazelnut-grey with light to dark tones. These particular types of stones were selected for their strong resemblance to the locally used sandstone in most rubble stone buildings in Northern Italy and Slovenia.

The masonry mortar was carefully designed with a granulometric distribution similar to those found in historic masonry buildings [26] with a hydraulic lime to sand ratio of 1:7 by mass. The grain size distribution of the aggregate ranged between 0.05 and 3 mm, and about 45 % of sand had a size smaller than 0.5 mm. The mortar was regularly sampled and tested after at least one month of air curing, to determine the flexural tensile strength, measured through three-point-bending tests on prismatic specimens (160 × 40 × 40 mm) according to EN 1015–11 [27], the compressive strength of mortar, measured on prism halves obtained from bending tests; the indirect tensile strength (splitting tests), measured on cylindrical samples (nominal height 200 mm, diameter 100 mm) according to EN 12390–6 [28]. The main results are summarized in Table 1.

The average specific weight of dry masonry was about 21.0 kN/m^3. This value was estimated based on the specific weight of mortar and stones, along with the volume of a small portion of masonry taken

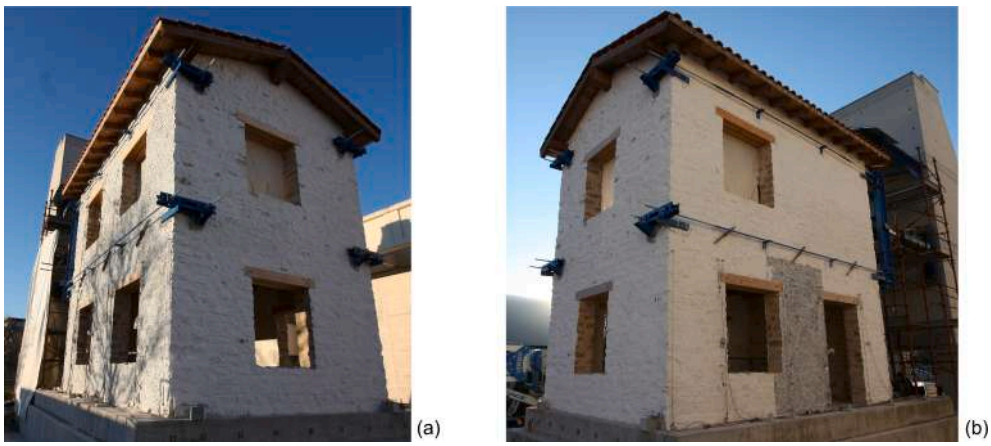

Fig. 1. Views of the building from outside: (a) East and North walls; (b) North and West walls.

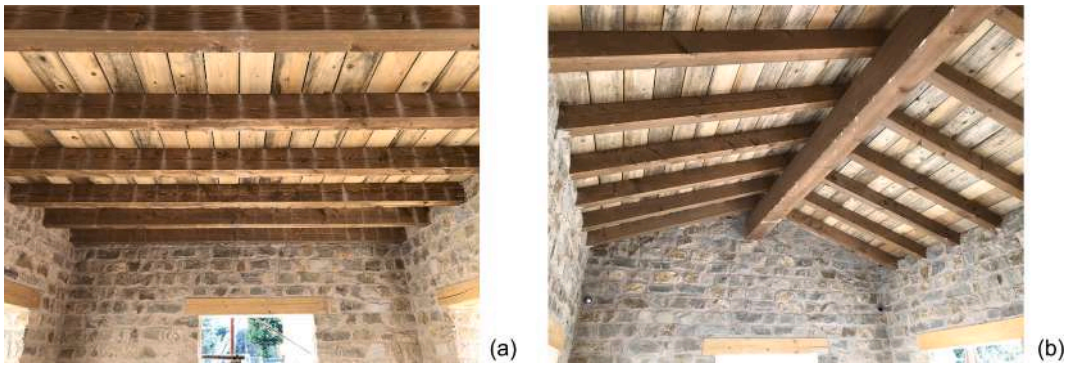

Fig. 2. Views of the building from inside: intrados of the intermediate floor (a) and of the roof (b).

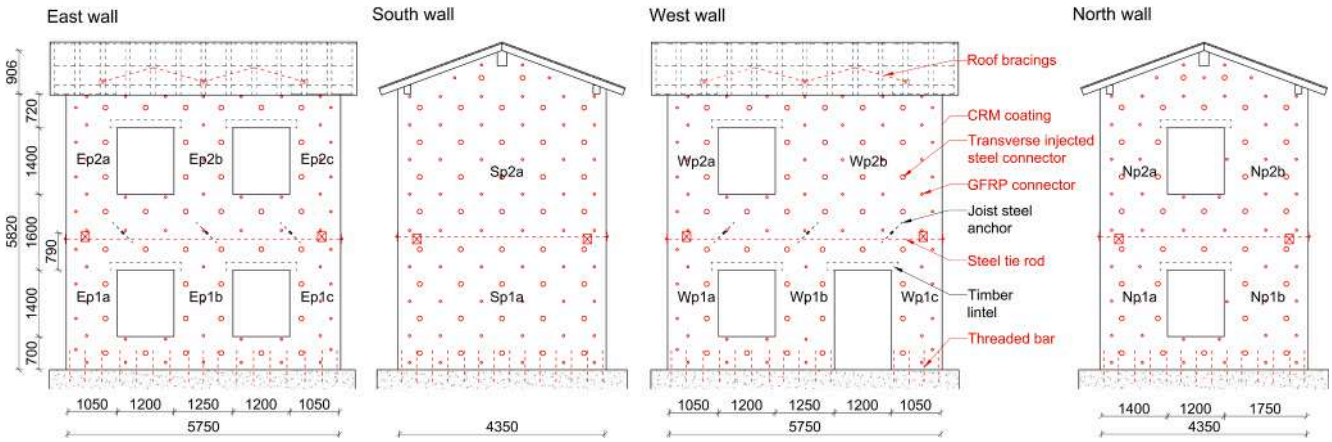

Fig. 3. Side views of the building and coating connection details (dimensions in mm).

during the construction of the building. The compressive strength of masonry was evaluated through uniaxial monotonic compression tests conducted on three masonry specimens. The specimens had a height of 1100 mm and a cross section of 650x350 mm. The tests resulted in a mean compressive strength of 1.49 MPa (CoV = 16.8 %).

The walls of the building were connected to the foundation by 120x150x150 mm reinforced concrete blocks (teeth) embedded within the wall thickness to prevent potential sliding at the masonry-concrete interface. The small blocks were anchored into the reinforced concrete (RC) foundation by 16 mm diameter steel bars. This was to simulate existing buildings, which typically have masonry foundations and cannot slide at contact with the foundations.

The intermediate wooden floor (Fig. 2a) consisted of solid timber joists (cross-section of 120 × 160 mm^2, 3950 mm length) spaced at 600 mm, located into masonry pockets providing a support length of 150 mm. To represent planks typically used in historical constructions of Northern Italy [29], 25 mm thick timber boards were nailed to the floor joists. Three of the floor joists were connected to the East and West walls by means of steel anchors, 1800 mm spaced, passing through the masonry wall, and clamped by a steel wedge (Fig. 1a,b; Fig. 5a). The anchors were fastened to the floor joists through a plate using three wood screws per plate. The wooden pitched roof (Fig. 2b) consisted of 533 mm

Fig. 4. Typical view of the horizontal cross-section of the stone-masonry walls during construction;

Table 1
Mechanical properties of the mortar (*CoV* = coefficient of variation).

Property of masonry mortar	n° of samples	Mean [MPa]	*CoV* (%)
Flexural tensile strength	5	0.57	8.8
Compressive strength	6	1.54	11.7
Indirect tensile strength	5	0.75	13.3

spaced solid timber joists (cross-section of 100 × 140 mm^2), connected at one end to a solid timber ridge beam (cross section of 200 × 320 mm^2). The opposite end was laid on the longitudinal walls. The roof was covered with 25 mm thick timber board planks, which were then overlaid with fired clay tiles. A couple of parallel wooden lintels (cross-section of 170 × 170 mm^2, 1500 mm length) was laid above each opening, provided with an end support of 150 mm on each side. All wooden elements were made of red spruce, with an average specific weight of 4.5 kN/m^3.

3. Retrofitting technique

The adopted retrofitting approach consists of different interventions aiming at promoting the "box behaviour" [30] of the building and improving the seismic resistance of the walls. To achieve the "box behaviour", the out-of-plane mechanisms must be first prevented. To this end, the test building was first provided with the longitudinal steel tie rods (Fig. 3), located at the first-floor level, and the steel anchors (Fig. 5a), frequently already present in existing masonry buildings, thus they were installed since the beginning of the first test. As discussed in the following, after testing the unstrengthened building, steel cable "X" bracings were also connected to the joist of the roof to improve its in-plane stiffness and further promote the global behaviour of the building. Finally, a series of techniques were used to improve the in-plane resistance and mutual interlocking of masonry walls. In more detail, the walls were repaired by injecting the cracks with low-viscosity cementitious mortar to a depth of approximately 50 mm. Moreover, transverse injected steel connectors 16 mm diameter were installed (50 mm total diameter) and a layer of a CRM coating (nominal thickness 30 mm) was applied on the outer surface of the perimeter walls to improve their lateral capacity." (Fig. 5b). The blind hole for the injected steel connector had a depth of 50 mm lower than the masonry thickness, to avoid interventions inside the building. The GFRP mesh embedded within the coating had a 66x66 mm^2 grid dimension and was composed of twisted fiber wires in the warp direction weaved on parallel fiber wires in the weft direction (dry fiber cross section 3.8 mm^2). Tensile tests were carried out on the GFRP wires to determine the tensile strength and axial stiffness, according to EAD-340392 [31] and ISO 10406-1 [32] and are summarised in Table 2.

The GFRP mesh, produced in 2000 mm wide rolls, was applied to the four external facades of the building by ensuring an overlapping between adjacent strips of about 132 mm (i.e. two grid spacings). Moreover, along the four vertical corners of the building, GFRP angular mesh elements, with a 66x66 mm grid dimension and a width of 330 mm, were added to guarantee the continuity of the reinforcement at the walls' intersections. No angular elements were installed at windows' corners as the GFRP sheets were cut and placed so that the horizontal and vertical bars of the mesh resulted placed sufficiently close to each corner to effectively reduce the risk of diagonal crack formation. This decision was taken to simplify the procedure and limit its invasiveness.

The coating was anchored to the walls by GFRP L-shaped connectors (4/m^2) and transverse injected steel connectors (2/m^2), following the arrangement reported in Fig. 3.

The L-shaped connectors were inserted into 16 mm diameter holes drilled in the masonry, for a depth of 300 mm, and injected with a vinyl ester epoxy resin as in Fig. 6a. The connectors had a cross-section of 7 × 10 mm^2, and a nominal dry fiber cross-section equal to 32.4 mm^2; they had a nominal characteristic tensile strength of 17 kN and an ultimate strain of 1.9 %. In front of each connector, a GFRP mesh sheet (150 × 150 mm) with a 33x33 mm grid dimension was positioned to distribute stresses within the coating.

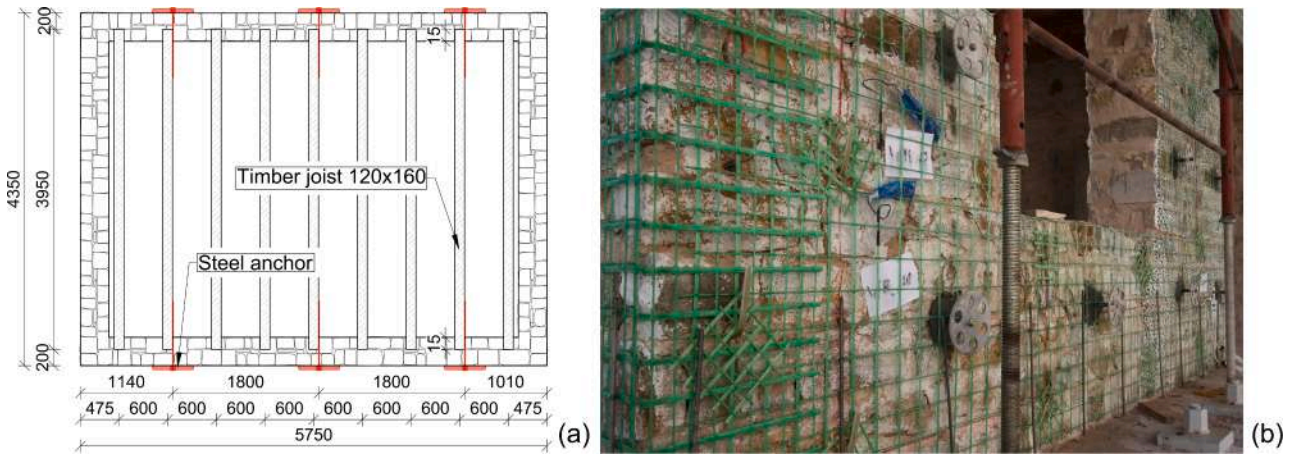

Fig. 5. (a) Plan view of the steel anchors layout (dimensions in mm); (b) GFRP mesh and anchors just before the application of the mortar coating. Note the additional angular elements at the corner, the GFRP connectors, the head washers of the transverse injected steel connectors and the anchor bars with the foundation.

Table 2
Properties of the GFRP wires.

Property	Number of samples	Mean	COV (%)
Twisted mesh wires – 66 × 66 mm^2 mesh pitch			
Nominal dry fiber cross section A_{fib} (mm^2)	–	3.70	–
Tensile resistance T_w (kN)	6	6.37	4.6
Ultimate strain ε_u (%)		2.29	3.5
Axial stiffness EA_{fib} (kN)		280.4	3.8
Parallel mesh wires – 66 × 66 mm^2 mesh pitch			
Nominal dry fiber cross section A_{fib} (mm^2)	–	3.70	–
Tensile resistance T_w (kN)	10	6.42	3.8
Ultimate strain ε_u (%)		2.21	4.3
Axial stiffness EA_{fib} (kN)		292.8	3.5

The transverse injected steel connectors were made with a 16 mm diameter threaded stainless steel bar, 365 mm long, centered in a 50 mm diameter hole and embedded in a high resistance thixotropic cement-based mortar (Fig. 6b). The holes were drilled by using a water-cooled core drilling machine. The transverse connectors had the important role of connecting the wythes of the wall and also anchoring the CRM system. To connect the mortar coating to the transverse connectors, perforated stainless steel washers (4 mm thick), with a nut welded at the center, were screwed on the head of the threaded bar, at a half thickness of the CRM coating, above the GFRP mesh.

For the mortar coating, a natural hydraulic lime mortar was used, whose mean mechanical properties are summarized in Table 3. Besides the evaluation of the flexural and the compressive strength of prisms and the indirect tensile strength of cylinders (according to procedures mentioned in §2 for the masonry mortar), the compressive strength and Young's modulus were evaluated on cylindrical samples (nominal height 200 mm, diameter 100 mm), according to EN 12390-3 [33] and EN 12390-13 [34]. The mortar for coating was regularly sampled and tested after at least two months of air curing. The average specific weight of the mortar was about 18.0 kN/m^3. Before applying the CRM coating, the mortar in masonry joints was removed for a depth of 10 mm and the masonry surface was washed with a high-pressure water cleaner. The washing removed the dirt, paint and moistened the masonry surface, which promoted a better adhesion of the CRM coating. The white paint was applied on the façade to make the detection of cracks easier during the test on the unreinforced building.

To increase the in-plane flexural resistance of the walls, the CRM coating was anchored to the foundation by 8 mm diameter stainless steel threaded bars (characteristic yield strength 200 MPa). The bars were anchored 250 mm deep into the RC foundation by epoxy resin, and 400 mm into the coating (Fig. 6c). The bars were distributed along the entire perimeter of the building, three per meter, at about 10 mm from the masonry wall surface. The bars were installed beneath the GFRP mesh to avoid possible splitting failure mechanisms of the mortar coating. Previous pull-out tests [35], carried out on 6 mm diameter threaded steel bars showed that an approximate length of 50 times the diameter is enough to anchor the bars in the reinforced mortar coating.

Walls were connected by four additionally installed high strength steel rods (Class 8.8, 22 mm diameter threaded bars), placed along the internal surface of the perimeter walls, below the intermediate floor joists. They were anchored by 150x150x15 mm ribbed steel plates on the surface of the coating. At the roof level, eight tightened steel cable bracings (8 mm diameter) were installed on the timber rafters, in a "cross" configuration to increase the in-plane roof stiffness.

Note that no interventions were adopted to increase the in-plane stiffness of the timber floor, which remained flexible during both tests. However, the results of the cyclic tests together with the dynamic characterization discussed below, revealed that the adopted retrofitting intervention was able to promote the box response of the building, even without the adoption of devices to increase the floor stiffness.

4. Test setup

4.1. Loading layout

The test setup is depicted in Fig. 7. The lateral load (V_b) is applied by means of two hydraulic servo-controlled actuators (capacity 1500 kN each) installed on a reaction RC wall. One actuator is applied on the East

Table 3
Mechanical properties of the mortar of the coating (*CoV* = coefficient of variation).

Property of the mortar of the coating	n° of samples	Mean [MPa]	*CoV* (%)
Flexural tensile strength	6	3.44	4.2
Compressive strength	6	15.27	10.9
Compressive strength on cylinders	5	13.11	4.78
Indirect tensile strength	3	1.73	12.84
Modulus of elasticity	5	10,091	2.66

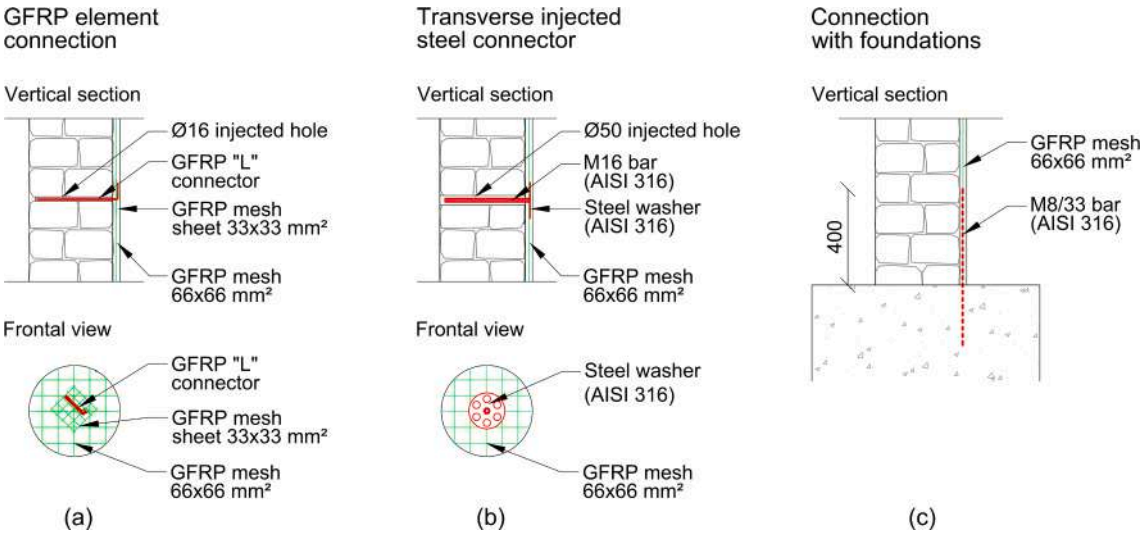

Fig. 6. Details of the retrofitting intervention: connection to the wall with (a) GFRP elements, (b) transverse injected steel connectors and (c) connection to the foundation by steel bars.

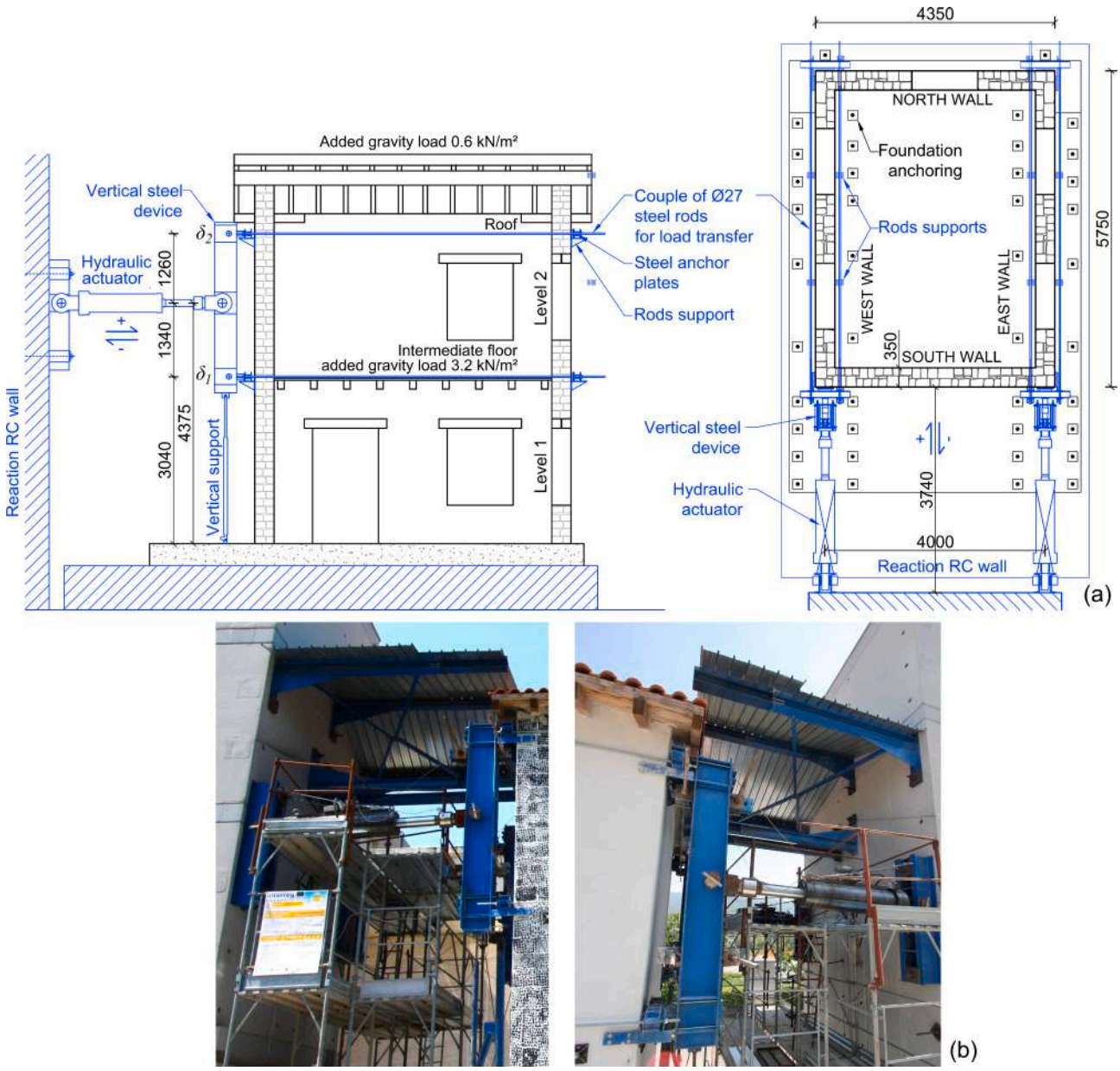

Fig. 7. Loading apparatus: (a) schematics section and plan view (dimensions in mm); (b) actual view.

wall and the other on the West wall. The load applied by each actuator was subdivided between the intermediate floor and the roof through a vertical steel beam hinged to the actuator, so that 51 % of such force was applied at the top of the first level and 49 % at the top of the second level of the building. This distribution was proportional to the product of the floor mass with the corresponding floor level.

The loading apparatus was located on the South side. When loading from the South to the North (positive loading direction), the actuator forces pushed against the South wall; when loading in the opposite direction (negative loading direction), the forces pulled on the North wall corners. The lateral force was transferred from the South to the North by four pairs of steel rods (27 mm diameter) placed at the sides of the two longitudinal walls, which were anchored at each end by a steel anchor plate. A gap was provided between the steel elements and the masonry to avoid undesired longitudinal constraints for the walls.

The maximum displacement capacity of the testing apparatus was 150 mm in both loading directions.

The self-weights of the intermediate floor and the roof were equal to 0.2 kN/m^2 and 0.8 kN/m^2, respectively, considering a floor area equal to 4000 × 5400 mm^2 and a roof area of 5400 × 6500 mm^2. A total of 162 concrete blocks with dimensions 150 × 150 × 600 mm were placed on the intermediate floor and 55 × 120 × 250 mm clay bricks on the roof to simulate the typical combination of vertical loads required by the Italian structural code for seismic conditions [36]. These additional blocks and bricks were uniformly spread over the floor/roof area. The total loads per unit area (i.e., self-weight and added load) applied on the intermediate floor and roof were 3.4 kN/m^2 and 1.4 kN/m^2, respectively. Note that the total area of the roof, which was considered in the calculation of the applied loads, was higher (i.e., 37.4 m^2) than that of the first floor (i.e., 21.6 m^2).

The vertical stress at the base of the building was expected to range from a minimum of 0.16 MPa (South wall) to a maximum of 0.22 MPa (East wall) and on the intermediate floor, from 0.08 MPa to 0.11 MPa.

4.2. Instrumentation

The instrumentation used for the tests is shown in Figs. 8 and 9. It consists of 52 displacement transducers, 2 load cells, 6 accelerometers

and 2 camera setups for the DIC (digital image correlation) measurements. Two displacement transducers (HW, HE) with a stroke of 950 mm and two 1000 kN capacity load cells (CW, CE) were installed on the actuators to detect the pistons' stroke and the applied forces. Moreover, horizontal displacement transducers (H1SW, H1SE, H2SW, H2SE) with a stroke of 75 mm and four 1000 kN capacity load cells (C1SW, C2SW, C1SE, C2SE) were applied in each of the four loading areas of the South wall, to survey the lateral displacements of the building and the load distribution at the intermediate floor and the roof. The horizontal (BSW, BSE, BNW, BNE) and vertical displacements (V1W, V13W, V19E, V33E) at the base corners were also monitored. Many other linear potentiometers (100 mm stroke) were installed on masonry piers and spandrels, to check vertical and diagonal displacements and the activation of cracks since the very early stages of the tests.

The natural frequencies, mode shapes, and damping factors of the building were determined through a modal identification method for output-only systems. This method employed frequency domain decomposition as outlined in [37,38]. The investigation was carried out for four distinct configurations: the unreinforced masonry (URM) building prior to testing, the URM building post-testing, the retrofitted masonry (RM) building before testing, and the RM building after testing.

For the experimental process, six seismic accelerometers were positioned across two experimental setups that shared four reference sensors. The instruments effectively captured ambient-induced vibrations caused by external factors such as traffic and wind to allow for the estimation of the rigid body motions of the four walls at both the first floor and roof level, as shown in Fig. 9. Data acquisition was performed in the horizontal plane, in the transverse direction of the walls. The temporal data were sampled at a frequency of 300 Hz, with each measurement session having a minimum duration of 40 min.

DIC systems were installed to measure displacements and crack formation on the entire surface of the East wall façade and a portion of the West wall. This type of measuring system can be used for several purposes, as reported in Oats et al. [39], but it is particularly useful for masonry elements because it allows the detection of cracks in the early stages when the damage cannot be seen by the naked eye. In Howlader et al. [40], the same methodology has been adopted for in-plane tests on masonry walls. The high accuracy that can be reached is discussed, also analysing the ideal step size to guarantee an accurate data extraction.

Before the test, the surfaces were rendered visually regular with white paint, made with water and hydraulic lime powder. Then, a random black speckle pattern was applied to allow the software to detect the surface. A high-resolution camera (45.7 Megapixels) automatically shot with constant time intervals, and the maximum displacement (in positive and negative load directions) was captured manually. The outputs were plotted as major strain views of the measured area (Figs. 11a,b and 14a,b).

4.3. Test protocol

The building was tested under quasi-static displacement load controls, to simulate earthquake load. Such a test guarantees a good correspondence of the damage to what can be expected in an actual seismic event since, usually, the fundamental vibration mode of the building involves most of its mass and its deformation increases along the structure height. Moreover, quasi-static testing gives insight into the hysteretic response, dissipated energy between cycles and damage evolution. Also, some previous experimental studies on buildings [41] and walls [42] have shown that quasi-static cyclic testing usually provides a more demanding environment than a dynamic excitation simulating a seismic event.

In the tests, the horizontal displacement at the roof of the building was gradually increased, and each displacement amplitude was repeated twice in both directions. The experiments were controlled through a computer software, so that both actuators simultaneously reached the same top displacement at West and East walls. The net structure displacement at the top was calculated using the following relation (with reference to the instruments as indicated in Fig. 8).

$$\delta_2 = \frac{(H2SE + H2SW) - (BSE + BSW)}{2} \tag{1}$$

Also the net lateral average displacement of the first floor, δ_1, was continuously surveyed during the test:

$$\delta_1 = \frac{(H1SE + H1SW) - (BSE + BSW)}{2} \tag{2}$$

Unlike δ_2, the displacement δ_1 was not directly controlled, and its value depends on the structure's response.

The first test, on the unreinforced masonry (URM) structure, was stopped close to the ultimate limit state when the damage was significant but repairable. Then, the repair and strengthening operations were carried out. The second test on the retrofitted masonry (RM) structure, was carried out up to near collapse. The loading cycles are presented in Fig. 10.

5. Experimental results

The global response of the buildings was evaluated through the capacity curves representing the total lateral load (V_b) against the net lateral roof displacement δ_2 (Eq. (1)). The building drift (γ_2) was

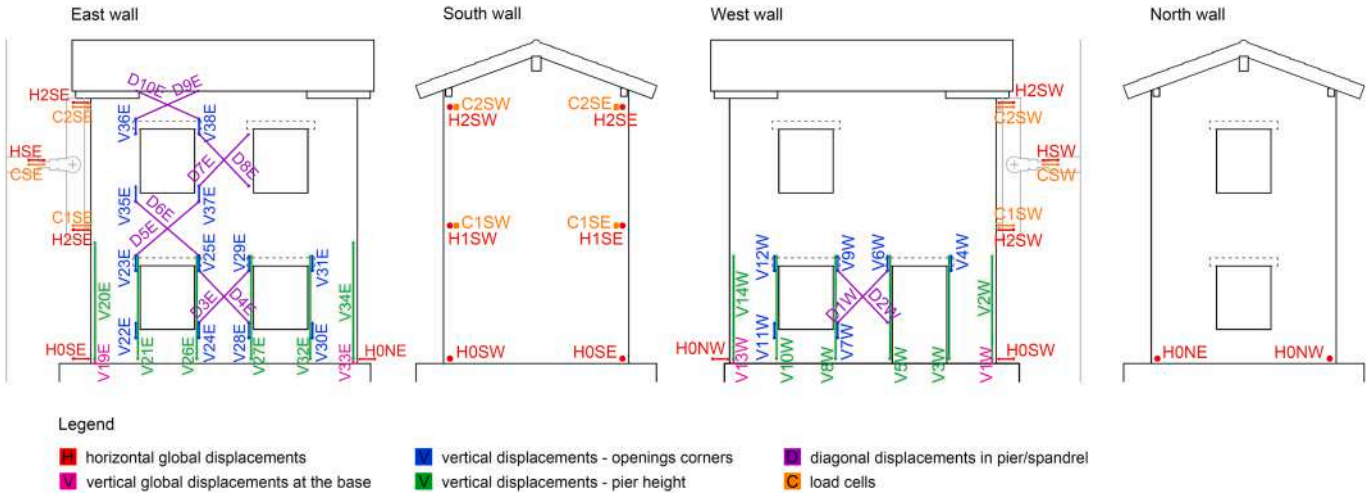

Fig. 8. Load and displacement transducer set-up.

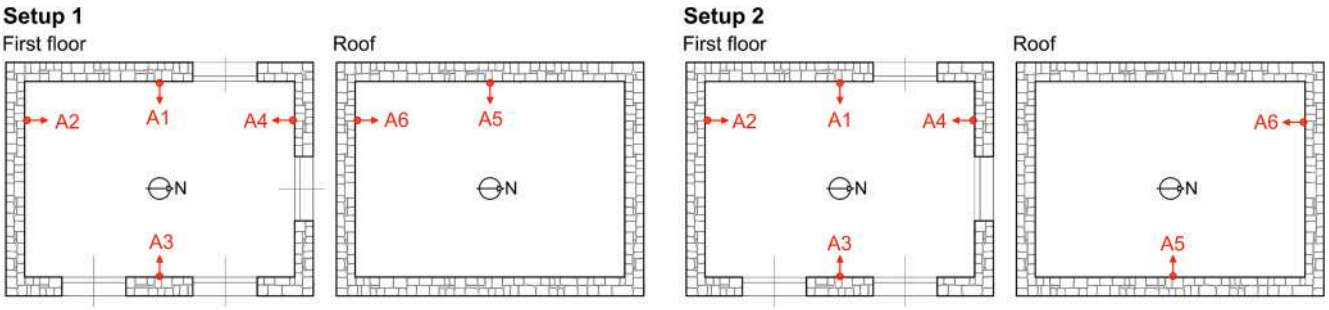

Fig. 9. Accelerometer set-ups.

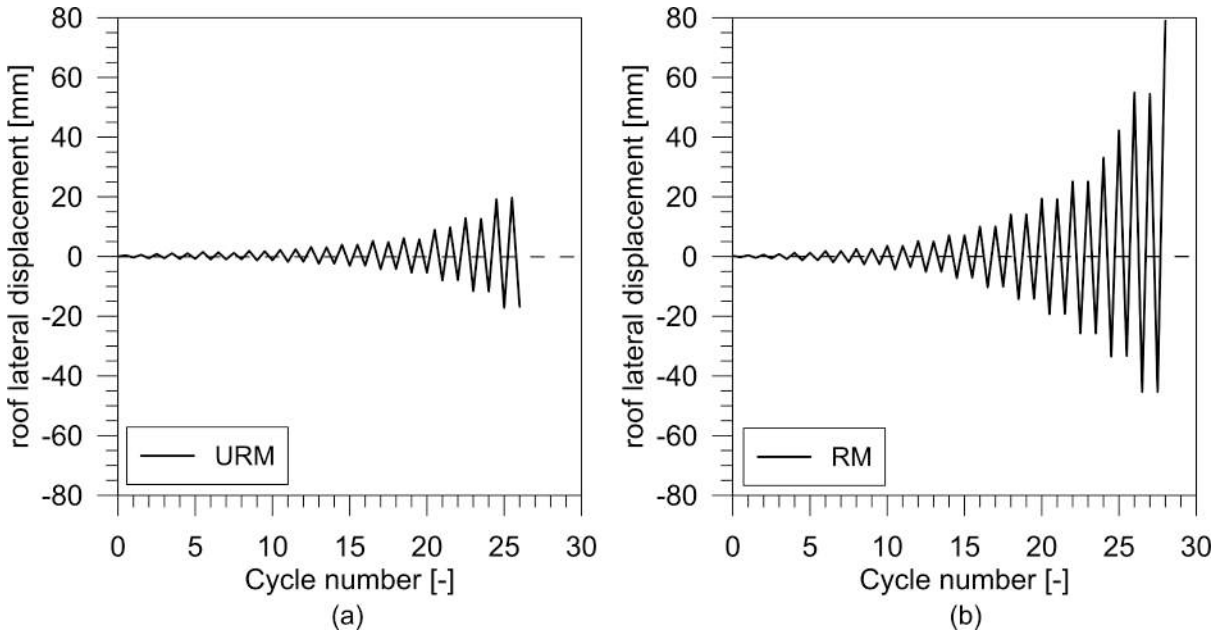

Fig. 10. Loading cycles for the (a) unreinforced structure test and (b) for the retrofitted one.

determined by dividing δ_2 by the wall's height from the foundation, equal to 5640 mm (Fig. 7). The drift at the intermediate floor (γ_1) was determined by dividing δ_1 (Eq. (2)), by the height from the foundation, equal to 3040 mm.

The behaviour of the URM and RM buildings is described in the following subsections, in terms of capacity curves and damage evolution. Two groups of cracks were generally distinghushed: the horizontal cracks at the ends of the piers and vertical cracks at the end of spandrels

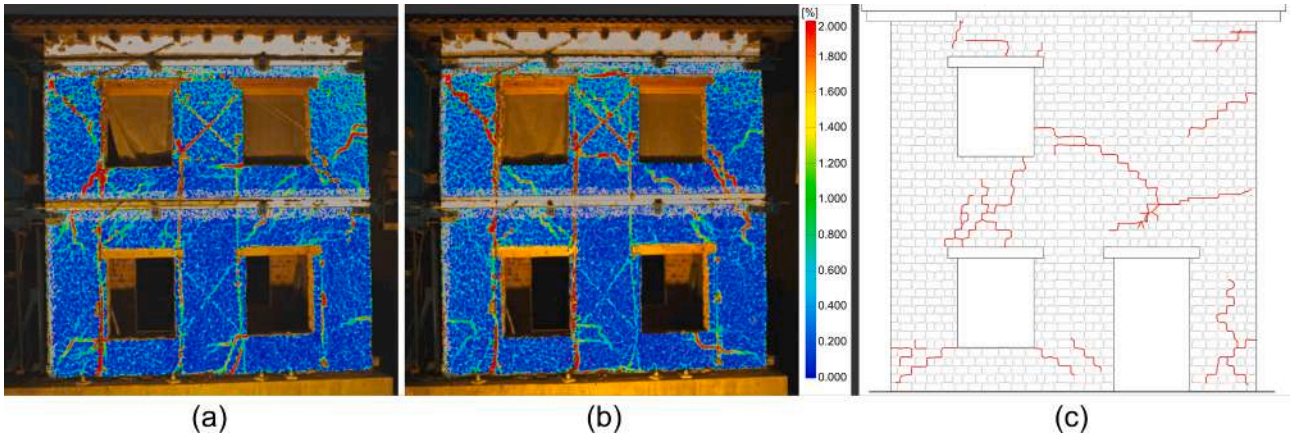

Fig. 11. URM building cracks (maximum strains) on the East wall at the end of the test, detected by the DIC System for negative N-S (a) and positive S-N (b) loading directions, and crack configuration on the West wall (c).

were related to the activation of the in-plane bending failure, whereas diagonal cracks within piers and spandrels related to the in-plane shear mechanism.

5.1. URM building

The URM building was tested about six months after its construction. The crack pattern at the end of the test is illustrated in Fig. 11. In more detail, in Fig. 11a,b are shown the maximum strains of the East wall detected with the DIC system, whereas Fig. 11c reports a sketch of the cracks directly surveyed on the West wall. Note that the path of the cracks followed mainly the mortar joints.

The significant events that occurred during the test of the URM building are summarized in Table 4 and the experimental load–displacement curves, V_b-δ_2 and V_b-δ_1, are illustrated in Fig. 12a, b. The curves are almost linear until the first flexural cracks occurred at the top and bottom of the pier Ep2b (see id. in Fig. 3 for location), for a total lateral force V_b of about +66 kN. At the attainment of $\delta_2 = +1.2$ mm, the stiffness of the building gradually started to reduce, as cracks developed close to the corners of openings on the first and second level and horizontal cracks occurred at the top of the pier Ep2a. A further reduction of the lateral stiffness was caused by visible diagonal shear cracks on the West and East wall spandrels above the windows of the first level ($\delta_2 = +2.1$ mm). One of these cracks formed above the door and then extended to the window's corner of the second level. With increasing lateral displacements, shear cracks formed on piers Ep2a and Ep2b, and the building attained the maximum capacity, equal to +267 kN. Then, the force slightly decreased to +251 kN as the existing cracks further expanded (Fig. 13a). During the test, no building up-lift phenomena were observed at the base of the walls. The cracks at the first level were visibly thinner than those at the second level.

The transversal walls (South and North) exhibited some localized cracks around the loading points of the second level. Thin cracks also opened inside of the building, along the walls' intersections, evidencing a slight separation between orthogonal walls; moreover, a horizontal crack appeared at the base of the pier Np1b (Fig. 13b), related to out-of-plane bending, involving also a portion of the pier Wp1a.

However, as mentioned above, the most significant cracks developed in the longitudinal walls and were due to in-plane mechanisms affecting mainly the piers of the second level, thus demonstrating a structural response governed by a story mechanism at the second level.

Table 4
Summary of main test events of the URM building: base shear V_b, intermediate floor lateral displacement δ_1, roof lateral displacement δ_2, intermediate floor drift γ_1, building drift γ_2.

Event description	V_b [kN]	δ_1 [mm]	δ_2 [mm]	γ_1 [%]	γ_2 [%]
1. First flexural cracks at the top and bottom toes of the 2nd level pier Ep2b.	+66 −45	+0.22 −0.00	+0.85 −0.53	+0.007 −0.000	+0.015 −0.020
2. New cracks at the openings' corners; horizontal cracks at the top of pier Ep2a; beginning of a gradual stiffness reduction.	+84 −67	+0.43 −0.04	+1.21 −0.97	0.014 −0.001	+0.021 −0.017
3. Visible diagonal cracks in the East and West spandrels above the windows of the 1st level.	+125 −97	+0.88 −0.28	+2.14 −1.75	+0.029 −0.009	+0.038 −0.031
4. Attainment of maximum capacity; diagonal cracks in piers Ep2a, Ep2c.	+267 −256	+6.53 −7.71	+18.95 −16.60	+0.215 −0.254	+0.336 −0.294
5. Activation of story mechanism in the 2nd level.	+251 −239	+6.46 −7.87	19.58 −16.63	0.213 −0.259	0.347 −0.295

5.2. RM building

Four months after the URM test, the building was strengthened and then tested 32 days later. Some negligible, minor microcracks were detected around the openings, in the coating, likely due to shrinkage.

The crack pattern at the end of the test is illustrated in Fig. 14a,b (East wall) and Fig. 14c (West wall); the experimental capacity curve V_b-δ_2 is presented in Fig. 15, in black color. A summary of the significant events during the test is reported in Table 5.

The curve is almost linear until the first flexural cracks occurred at top and bottom of the piers of the first level, on the unreinforced wall side, at a displacement $\delta_2 = \pm 0.3$ mm. At almost $\delta_2 = +0.4$ mm, the stiffness of the building gradually started reducing, as cracks developed on the coating, close to the corners of the first level openings. With increasing lateral deflection, similar cracks occurred near the openings of the second level, while diagonal shear cracks appeared on the coating of the spandrels above the openings of the first level, causing a further reduction of the global stiffness. At about $\delta_2 = +3.2$ mm, the flexural cracks of the first level piers and the diagonal cracks of the spandrels began to spread locally and, contemporarily, diagonal shear cracks appeared in the piers. When exceeding $\delta_2 = +9.2$ mm, the cracks widely spread, causing a significant stiffness degradation. The maximum shear capacity was attained at +645 kN ($\delta_2 = +31.4$ mm) and −590 kN ($\delta_2 = -30.5$ mm). After the peak load, a graudal resistance decrease was observed. At $\delta_2 = -32.0$ mm, the first level piers suffered a significant opening of their cracks, promoting a sharp reduction of the global lateral stiffness in the subsequent cycles. Once a decrease in post-peak resistance of about 15 % was achieved, the test was conducted monotonically in the positive loading direction, up to near collapse. A sharp decrease of resistance from $V_b = +573$ kN to +509 kN occurred, as the GFRP mesh failed at the base of the piers Ep1b and Wp1a (Fig. 16a,b). Only two transverse injected steel connectors, located at half height of the piers Ep1b and Wp1b, were crossed by the diagonal cracks, but no wall leaves separation was detected. The pier Wp2b did not show any damage.

Close to the maximum displacement, a horizontal crack formed at the bottom of the piers Np1b and Wp1a, similarly to the URM test, causing a horizontal slippage of the North-West corner. In addition, some vertical splitting cracks occurred, from about $\delta_2 = +33.0$ mm, along the threaded bars connecting the CRM coating of the South wall to the building foundation. The vertical uplift at the South wall base detected by the instrument V1W was about +16.6 mm at the maximum top lateral displacement in the positive loading direction. Differently, in the negative one, the same instrument detected −1.21 mm. At the North wall base, the uplifts detected by the instruments V13W and V33E were about +5.73 mm and +1.94 mm respectively, at the maximum top lateral displacement in the positive loading direction. In the negative one, V13W and V33E measured about −0.85 mm and −0.61 mm, respectively.

Based on the damage propagation discussed above, it may be observed that the response of the structure was governed by a story mechanism involving the first level.

6. Comparison of results and discussion

6.1. Resistance, displacement capacity and stiffness

The maximum values of V_b, δ_1, γ_1, δ_2 and γ_2 obtained in the URM and RM building tests are summarized in Fig. 17. The effect of strengthening can also be assessed by comparing the hysteretic response of the two tests in Fig. 15, which show that lateral resistance increased by about 2.4 times, the displacement capacity became four times higher.

To evaluate the stiffness (K) degradation, the slope of the peak-to-peak line within the first loop performed at each displacement level of the V_b-δ_2 curves was calculated (Fig. 18a). In the URM building, the secant stiffness in the first cycle was 109 kN/mm and ultimately decreased to 14 kN/mm. The stiffness of the first cycle of the RM

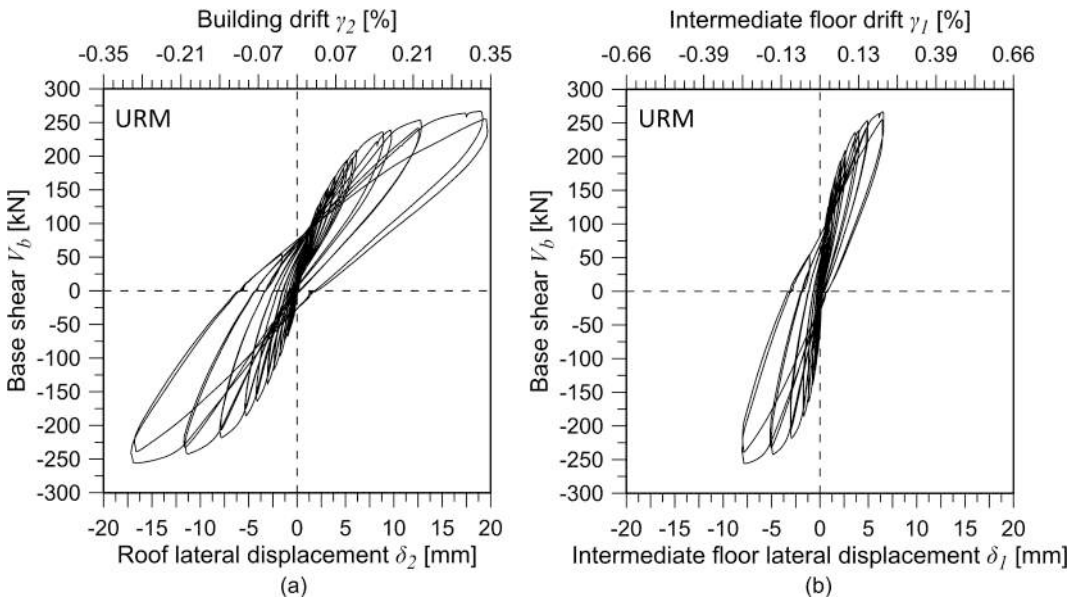

Fig. 12. URM: lateral load–displacement curves (a) V_b-δ_2 and (b) V_b-δ_1.

Fig. 13. Diagonal crack in the bottom right corner of pier Ep2a (a) and horizontal crack at the base of pier Np1b (remarked in black) (b).

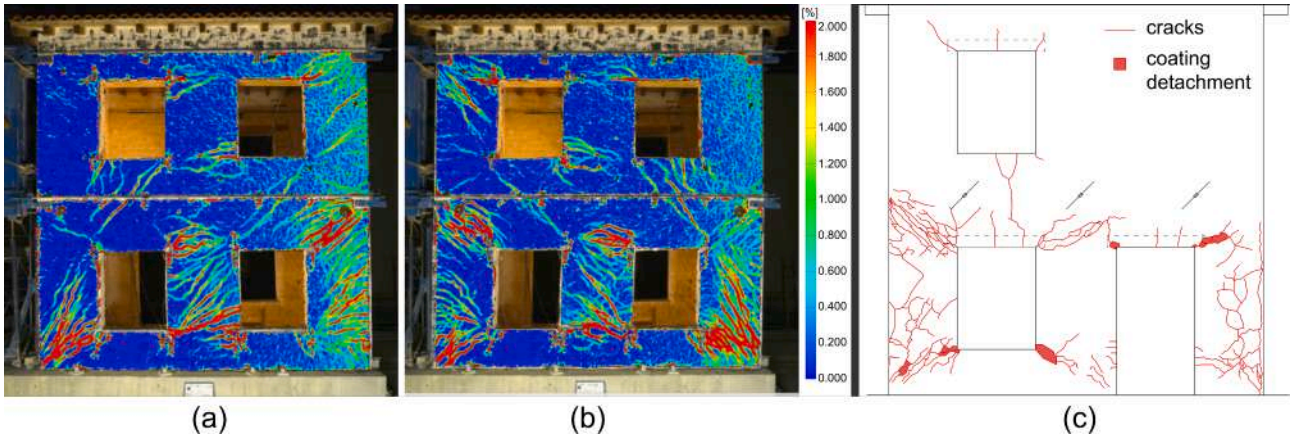

Fig. 14. RM building: cracks (maximum strains) on the East wall at the end of the test, detected by the DIC System for negative N-S (a) and positive S-N (b) loading directions, and crack configuration on the West wall (c).

building was 320 kN/mm; the progressive damage caused the reduction of the lateral stiffness up to a minimum of 11.7 kN/mm. The RM building's stiffness, in the first cycle, exceeded that of the URM building by 2.9 times.

In the URM building, the damage (shear and bending cracks) occurred mainly in the walls of the second level because of the low axial force and the flexural response of the piers. The coating changed the response mechanism of the structure since, in the RM building, the flexural failure mechanism is governed by the amount of vertical mesh wires for piers and horizontal wires for spandrels, making the resistances of the elements comparable between the first and second level. Thus, the failure occurred in the first level, where the lateral forces were higher.

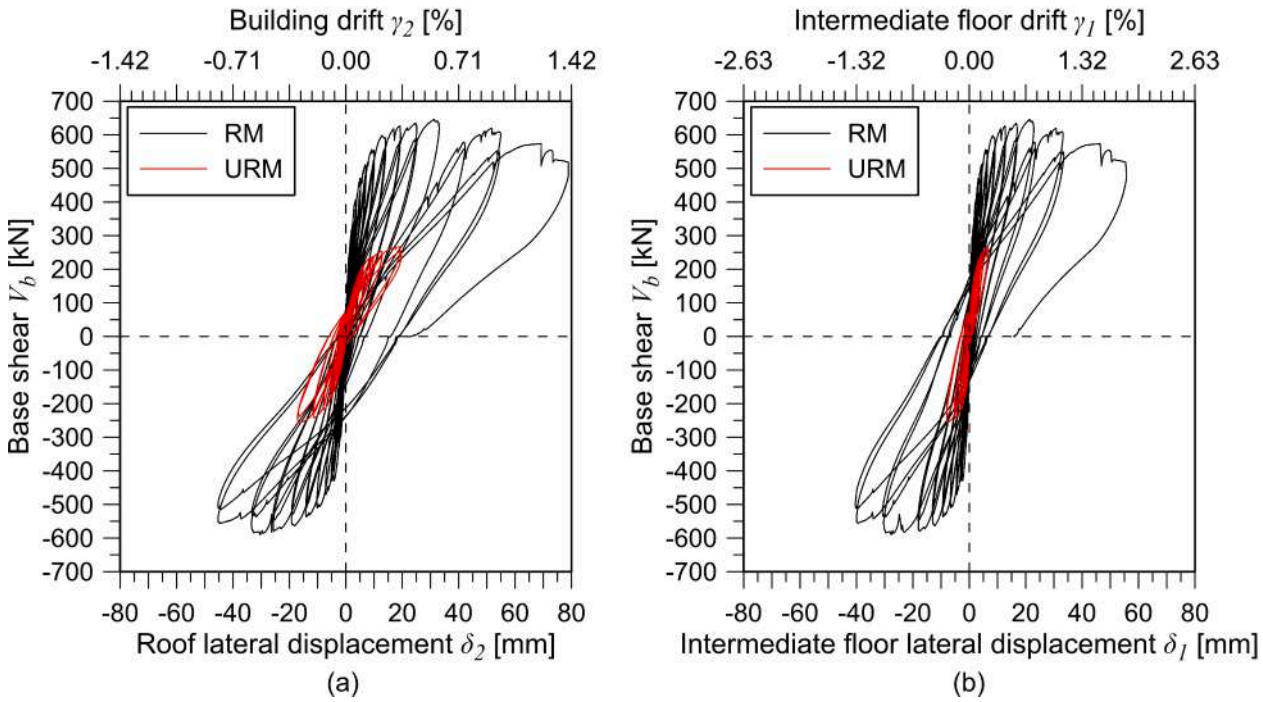

Fig. 15. RM: lateral load–displacement curves (a) V_b-δ_2 and (b) V_b-δ_1.

Table 5
Summary of main test events of the RM building: base shear V_b, intermediate floor lateral displacement δ_1, roof lateral displacement δ_2, intermediate floor drift γ_1, building drift γ_2.

Event description	V_b [kN]	δ_1 [mm]	δ_2 [mm]	γ_1 [%]	γ_2 [%]
1. First horizontal cracks in the piers at 1st level on the unreinforced wall side (East and West walls).	+112 −68	+0.21 −0.06	+0.30 −0.31	+0.007 −0.002	+0.005 −0.005
2. Cracks in piers, at the openings' corners at 1st level; start of a gradual stiffness decrease.	+129 −95	+0.27 −0.00	+0.40 −0.41	+0.009 −0.000	+0.007 −0.007
3. Cracks in piers, at the 2nd level openings' corners; diagonal cracks in the 1st level spandrels above the windows.	+249 −227	+0.75 −0.54	+1.20 −1.22	+0.025 −0.018	+0.021 −0.022
4. Spread of horizontal cracks in the coating of piers and diagonal cracks on spandrels. Shear cracks on 1st level piers.	+399 −391	+2.12 −1.79	+3.19 −3.31	+0.070 −0.059	+0.057 −0.059
5. Beginning of the uplift of the coating from the foundation in the South and North walls.	+419 −441	+2.60 −4.49	+4.10 −6.90	+0.086 −0.148	+0.073 −0.122
6. Wide spread of cracks in the coating of the 1st level piers and spandrels.	+556 −507	+5.77 −6.11	+9.14 −9.37	+0.190 −0.201	+0.162 −0.166
7. Attainment of maximum shear capacity.	+645 −590	+21.51 −27.76	+31.41 −30.50	+0.708 −0.913	+0.557 −0.588
8. Significant opening of the piers' cracks of the 1st level; abrupt decrease of the global lateral stiffness.	−537	−29.68	−31.95	−0.976	−0.566
9. GFRP mesh failure at the base of piers Ep1b and Wp1a.	+509	+46.88	+69.28	+1.542	+1.28

This change in behaviour can clearly be seen in Fig. 18b, where the displacements measured at the intermediate floor and at the roof are reported in different significant steps, for both URM and RM building: the larger displacements in the unreinforced structure occurred in the upper level, while in the reinforced structure the displacements of the lower level were more significant. In the URM building, the test was interrupted after reaching the maximum load. The first cracks were reached at the same displacement values for the URM and RM building.

The presence of the transverse steel injected connectors (density 2/m^2) was an effective solution to avoid the separation of wall leaves and to ensure the collaboration between the CRM coating and the masonry until the mesh rupture. The test on the reinforced building also showed the important role of the connections between the coating and the foundation, aimed at transferring tensile forces into the foundation and preventing significant vertical uplift and slip phenomena at the base.

6.2. *Vibration analysis*

The natural frequencies, mode shapes and damping factors of the building were evaluated for four different configurations: URM building, before and after testing, and RM building, before and after testing. The main results are reported in Table 6 and the different mode shapes are schematized in Fig. 19.

In the undamaged URM building, mode 1 was translational in the transversal direction (type "a" mode shape in Fig. 19) and mode 2 in the longitudinal one ("b"); mode 3 was rotational about the vertical axis ("c"); mode 4 described longitudinal walls oscillating out of plane in phase opposition ("d"); in mode 5 the longitudinal walls oscillate out of plane with floors in phase opposition ("e").

In the damaged URM building, the fundamental vibrating modes were inversed: modes 1 and 2 were translational in the longitudinal ("b") and transversal direction ("a"), respectively. Comparing with the undamaged configuration, the frequency of the mode shape "a" decreased by −14.9 % and that of "b" by −24.6 %. This is reasonably related to a stiffness degradation due to the damaging. The rotational mode about the vertical axis was not detected. Mode 3 described the out of plane oscillation of the longitudinal walls in phase opposition ("d"); in mode 4 the longitudinal walls oscillated out of plane, with floors in

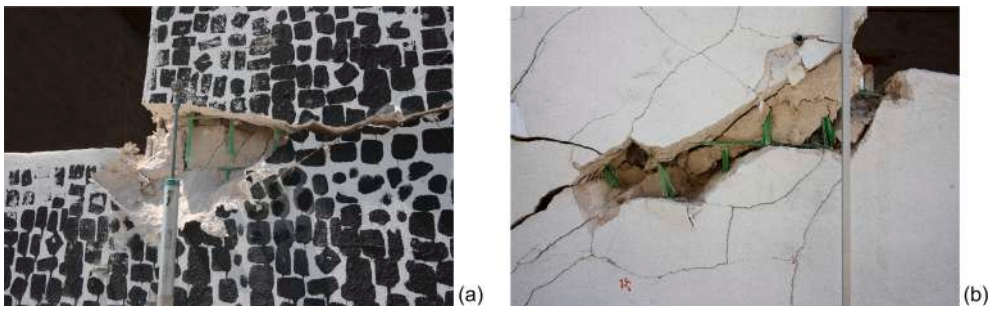

Fig. 16. Mesh failure at the bottom left corner of the pier Ep1b (a) and at the bottom right corner of the pier Wp1a (b).

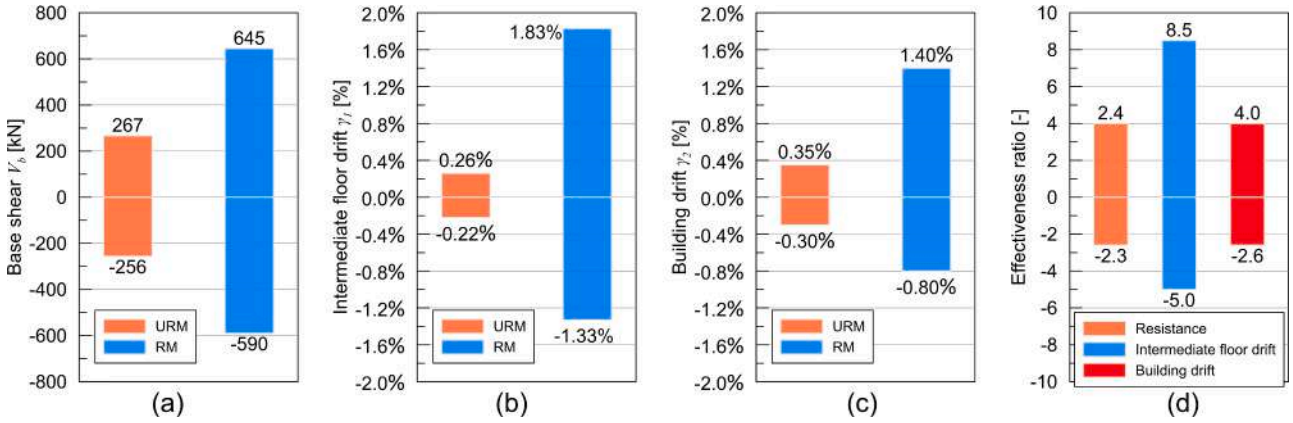

Fig. 17. Comparison between the URM and RM building: attained base shear V_b (a), intermediate floor lateral displacement δ_1 (b), roof lateral displacement δ_2 (c), and effectiveness ratio (d).

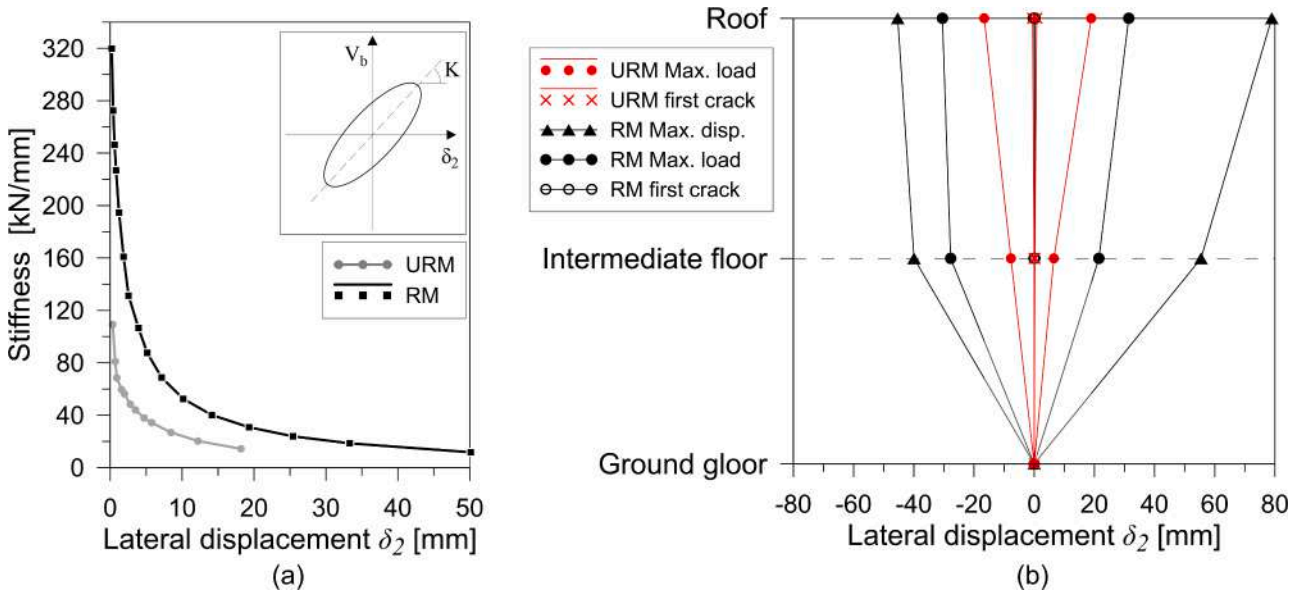

Fig. 18. URM and RM building: comparison in terms of (a) evolution of lateral stiffness and (b) deformed shape at different loading levels.

phase opposition ("e"). Mode 5 identified a local out of plane mechanism of the West longitudinal wall ("f").

Even though mode 5 could not be identified in the undamaged RM building, the mode shapes 1 to 4 were those of the undamaged URM building, with a frequency increase of at most 12 %. Thus, the retrofitting intervention did not significantly alter the vibration response of the original structure.

In the damaged RM building, modes 1 and 2 were translational in the longitudinal ("b") and transversal ("a") direction, respectively; mode 3 was rotational about the vertical axis ("c"); modes 4 and 5 were of type "d" and "e", respectively. As for the RM, the damage induced an evident frequency decrease. The change was −21.0 % with respect to the

Table 6
Natural frequencies, *f*, deformed shape id., with reference to Fig. 19, *DS*, and dampings, ξ_0, of the building, for the first five vibration modes.

Mode	Undamaged URM			Damaged URM			Undamaged RM			Damaged RM		
	f [Hz]	*DS*	ξ_0 [%]	*f* [Hz]	*DS*	ξ_0 [%]	*f* [Hz]	*DS*	ξ_0 [%]	*f* [Hz]	*DS*	ξ_0 [%]
1	10.38	a	1.6	8.692	b	1.6	11.63	a	1.1	7.84	b	2.3
2	11.53	b	2.1	8.834	a	2.4	12.89	b	3.6	9.186	a	1.2
3	12.52	c	0.8	13.2	d	0.8	13.38	c	3.3	11.52	c	3.3
4	15.26	d	0.9	14.13	e	0.9	14.77	d	3	13.74	d	0.9
5	16.68	e	1.7	17.95	f	1.7	–	–	–	15.77	e	1

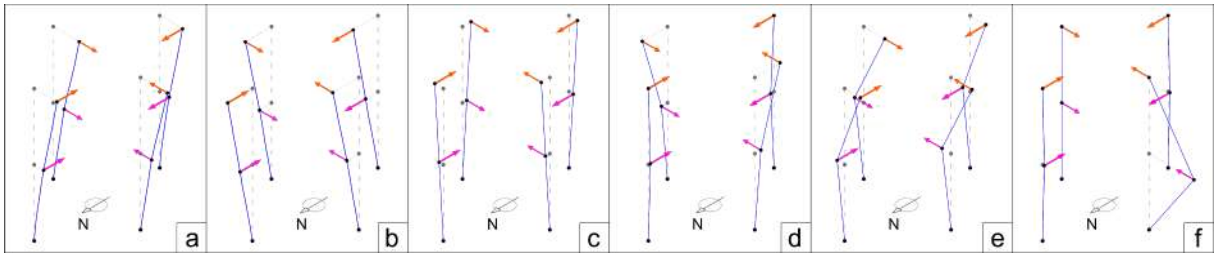

Fig. 19. Vibration mode shapes.

undamaged RM building, for the mode shape "a", and of −39.2 % for "b".

The vibration analysis also provided preliminary information on the damping capacity of the structure. Since the recorded environmental excitation was very low, the values of ξ_0 reported in Table 6 referred to the structure's initial, inherent viscous damping. In particular, the values related to the dominant vibration modes (1 and 2) were observed to fail within the range 1.1–3.6 %. These values align with those previously obtained in the literature for traditional stone masonry structures [17,43]. However, it was not possible to recognize a clear influence of damage or retrofit operations on the damping values.

6.3. Energy dissipation

To investigate on the energy dissipation capacity, the cumulative input energy was compared against the dissipated hysteretic energy. The cumulative input energy, E_{in}, was calculated as the cumulative work needed to deform the building from the beginning of the test to a specific value of displacement. For each loading cycle, it corresponds to the area under the positive and the negative branches of the hysteretic loop, which is represented by the brown dashed pattern reported in Fig. 20a ($E_{in,i}$). Similarly, the cumulative dissipated hysteretic energy, E_{hys}, was calculated as the sum of the areas ($E_{hys,i}$) included in each hysteretic loop (see the grey continuum pattern in Fig. 20a).

In Fig. 21a, the total and dissipated cumulative energy determined at each loading cycle are plotted as a function of the lateral roof displacement, δ_2, for the URM and the RM building. Table 7 presents the values of E_{in} and E_{hys} at resistance peak ($\delta_{V,max}$) and at maximum displacement (δ_{max}). The dissipative capacity of the RM building was significantly larger than that of the URM one ($E_{hys,RM}$ was 8.4 times higher at maximum displacement). This is because the cracks in the strengthened building spread widely across the walls, whereas in plain masonry, the cracks appeared only in a limited number of mortar joints. The high redistribution of internal stresses in the coating thus resulted in increased strength and deformation capacities.

The cyclic curves of both tests clearly evidenced that most of the input energy was dissipated in hysteretic loops through progressive damage and crack propagation, as evidenced in Fig. 21a, where the evolution of the E_{hys}/E_{in} energy ratios is reported. The hysteretic energy varied between 41 % and 53 % of the total input energy, for the URM building, and between 41 % and 64 %, for the strengthened building and tended to increase after the peak load. In the RM building, only the

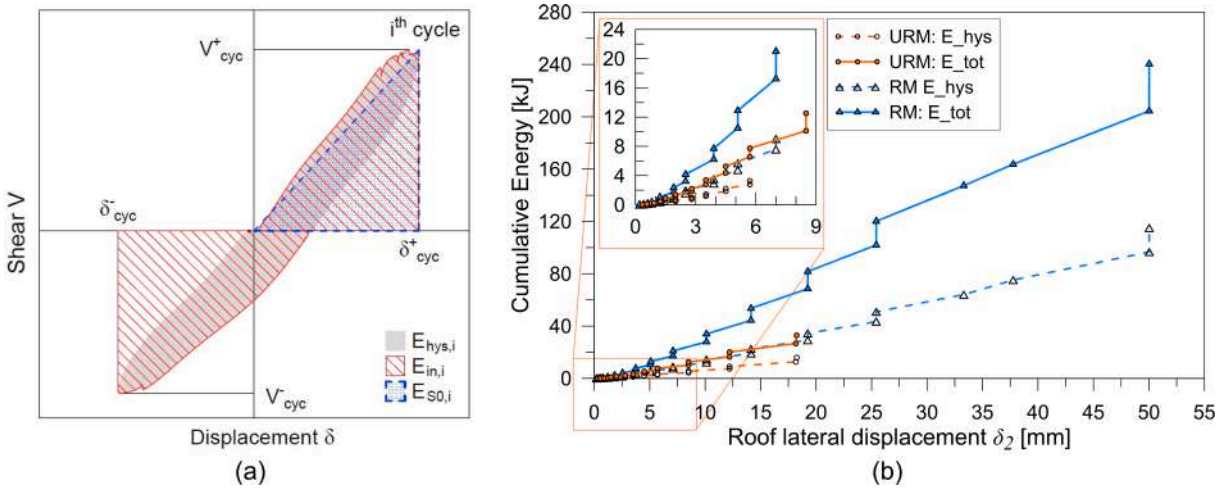

Fig. 20. (a) Schematization of input energy and dissipated hysteretic energy referred to a single base shear vs. displacement loading cycle; (b) comparison between the URM and RM building in terms of cumulative dissipated E_{hys} and total E_{in} energies.

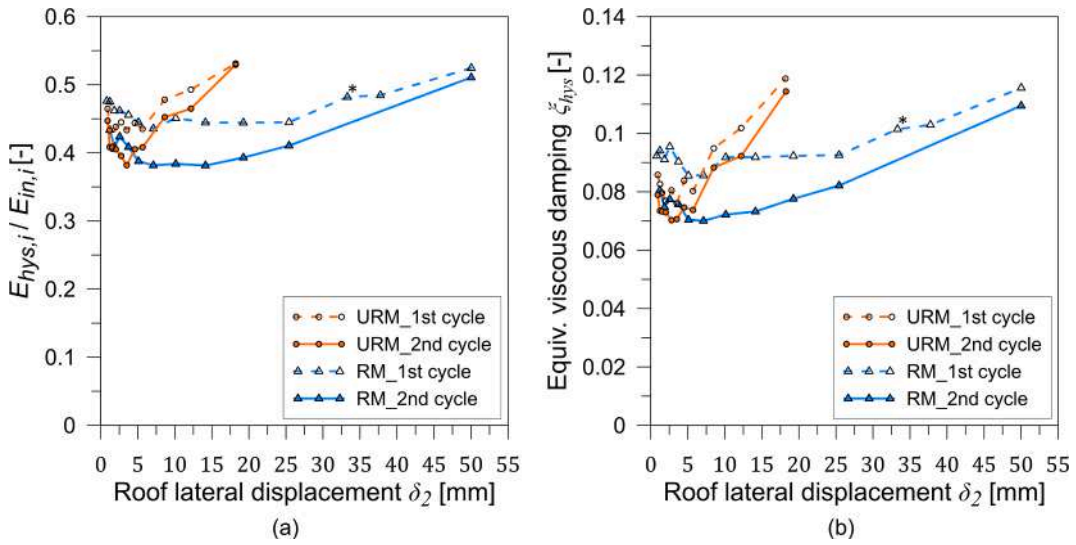

Fig. 21. Comparison between the URM and RM building in terms of (a) E_{hys}/E_{in} ratio, varying the lateral roof displacement δ_2 and (b) evolution of the equivalent hysteretic damping ratio ξ_{hys}.

Table 7
Values of cumulative input energy E_{in} and dissipated hysteresis E_{hys} at resistance peak ($\delta_{V,\max}$) and at maximum displacement (δ_{max}), for URM and RM.

Test	E_{in} [kJ]		E_{hys} [kJ]		E_{hys}/E_{tot}	
	$\delta_{Vb,\max}$	δ_{max}	$\delta_{Vb,\max}$	δ_{max}	$\delta_{Vb,\max}$	δ_{max}
URM	26.7	32.8	12.6	15.9	0.47	0.48
RM	146.4	288.6	61.6	133.7	0.42	0.46

positive half-cycle was considered for the determination of E_{hys} in the peak load cycle (±33.0 mm, * in Fig. 21a,b), due to an accidental disturbance on the measurement occurred in the negative half-cycle. This and the cycle after it were not repeated a second time.

6.4. Equivalent damping

An approximate value of the equivalent hysteretic damping of the structure can be then determined using the equation proposed by Chopra [44] and ATC FEMA 440 [45]:

$$\xi_{hys,i} = \frac{E_{hys,i}}{4\pi E_{s0,i}} \tag{3}$$

in which $E_{hys,i}$ is the hysteresis energy dissipated within each cycle and $E_{S0,i}$ is the strain energy associated with the secant stiffness of the structure in the i-th cycle, as illustrated in Fig. 20a (blue dashed pattern) and calculated by using equation (4).

$$E_{s0,i} = \frac{1}{2} \bullet k_{s,i} \bullet \delta_{max,i}^2 \tag{4}$$

being $k_{s,i}$ the secant stiffness of the i-th cycle (Fig. 18a) and $\delta_{max,i}$ the average between the positive and negative maximum displacements reached in the cycle.

The value of the equivalent hysteretic damping is used in many building codes [45,36] to evaluate the resisting ground acceleration of a building with the use of the Capacity spectrum method.

The curves of the base shear versus the roof lateral displacement δ_2 were considered for the determination of the equivalent hysteretic damping (Figs. 12a and 15a). The trends of the equivalent damping, calculated for the URM and RM building at the end of the first loading cycles, are reported Fig. 21b. The difference in ξ_{hys} among the two cycles was quite evident in the early stages. The gap reduced as δ_2 increased and after the peak load condition, ξ_{hys} almost coincided in the two cycles. Considering the initial cycles, the URM and RM specimens exhibited an initial hysteretic damping of about 8 % and 9 %, respectively, and maintained almost constant values till the attainment of the peak load. Then, ξ_{hys} tended to increase and, at the end of the test, reached about 12 % for both buildings. These values are comparable to those previously adopted by Gattesco and Boem [46], who considered ξ_{hys} of about 10 % for the ultimate limit state, both in the case of URM and RM buildings. Similar values were also obtained by Magenes [47] and Javed [48] for URM masonry.

7. Conclusions

The present study evaluated the performance of a 30 mm thick CRM coating applied only on the outer surface of a two-leaf rubble stone masonry building, to enhance its structural response under lateral loads. The CRM coating consisted of 66 × 66 mm^2 GFRP meshes embedded in a natural hydraulic lime mortar and was connected to the masonry through GFRP L-shape connectors. Moreover, to prevent the separation of the wall leaves and improve the anchoring of the coating, strong transverse injected steel connectors were used. The structure was subjected to quasi-static reverse cyclic loading using a displacement-controlled test protocol.

Based on the results of the tests, the following main concluding remarks can be drawn:

- As compared to the unstrengthened building (URM), the lateral resistance of the retrofitted structure (RM) was enhanced by approximately 2.4 times. Moreover, the displacement capacity and the total dissipated energy increased by approximately 4.0 times and 7.2 times, respectively. The results of this study also highlight that one-side application of a CRM system can effectively mitigate and delay the propagation of cracks in masonry under lateral loads of similar magnitude.
- In the URM building, the damage (shear and bending cracks) occurred mainly in the second level walls due to the low value of the axial load in the piers. On the contrary, in the RM building, the flexural resistance of the reinforced piers is mainly due to the CRM system, and thus, the collapse occurred at the first level, where the horizontal forces are higher. Moreover, the CRM coating promoted the activation of a "box behaviour" of the whole building that led to a kinematic mechanism involving the global overturning of the structure.

- Based on the current study and previous research [6], employing two transverse injected connectors per square meter was found to be an effective measure in preventing the separation of masonry leaves, as evidenced by the absence of wall bulging phenomena in the RM test. Also, the test on the repaired building evidenced the importance of the connection between the coating and the foundation. Proper connection details, such as vertical rebars, must be adopted to prevent vertical uplift phenomena and improve the global flexural capacity of the building.
- The evaluation of the equivalent viscous damping coefficient of the URM building ranged from 8 % to 12 % and was quite similar for the RM building. This information can be useful to evaluate the resisting acceleration with the use of the Capacity spectrum method.

Further experimental investigations are in progress to analyze the behavior of structural elements (piers and spandrels) to assess their deformation capacity before and after the strengthening. This information will be useful for calibrating numerical simulations in future studies aimed at defining reliable predictive models.

One of the authors, Eng. Allen Dudine, is a collaborator of Fibre NET s.p.a., which manufactures some products related to the research described in this paper. However, Eng. Allen Dudine had no influence over the data collection, analysis, or interpretation, and was not involved in the preparation of the manuscript. The other authors declare no conflicts of interest.

CRediT authorship contribution statement

Natalino Gattesco: Conceptualization, Investigation, Methodology, Writing – review & editing, Supervision, Project administration, Funding acquisition. **Emanuele Rizzi:** Investigation, Methodology, Data curation, Writing – original draft, Formal analysis, Visualization. **Ingrid Boem:** Conceptualization, Methodology, Writing – original draft, Visualization. **Luca Facconi:** Investigation, Resources. **Fausto Minelli:** Resources, Supervision. **Allen Dudine:** Resources. **Matija Gams:** Methodology, Investigation.

Declaration of Competing Interest

The authors declare that they have no known competing financial interests or personal relationships that could have appeared to influence the work reported in this paper.

Data availability

Data will be made available on request.

Acknowledgements

The experimental tests presented were carried out within the project CONSTRAIN, partially funded by the Interreg Italy-Slovenia Cooperation Program 2014-2020 and leaded by the University of Trieste (Italy), alongside with the University of Ljubljana (Slovenija) and the companies Fibre Net S.p.A., Igmat d.d., Veneziana Restauri Costruzioni S.r.l. and Kolektor CPG d.o.o.. The authors wish to extend their sincere thanks to Eng. Michele Dilena from the University of Udine for his invaluable contribution to the post-processing of the vibration analysis data. The authors would also like to express their gratitude to Eng. Sara Verza and Eng. Alessia Bez from the University of Trieste and to Eng. Veronika Pučnik from the University of Ljubljana for their contribution in executing the tests and analysing the resulting data. Their assistance is deeply appreciated.

References

[1] Kouris LAS, Triantafillou TC. State-of-the-art on strengthening of masonry structures with textile reinforced mortar (TRM). Constr Build Mater 2018;188:1221–33. https://doi.org/10.1016/j.conbuildmat.2018.08.039.
[2] Gattesco N, Amadio C, Bedon C. Experimental and numerical study on the shear behavior of stone masonry walls strengthened with GFRP reinforced mortar coating and steel-cord reinforced repointing. Eng Struct 2015;90:143–57. https://doi.org/10.1016/j.engstruct.2015.02.024.
[3] Corradi M, Borri A, Poverello E, Castori G. The use of transverse connectors as reinforcement of multi-leaf walls. Mater Struct 2017;50. https://doi.org/10.1617/s11527-016-0977-3.
[4] D'Antino T, Carozzi FG, Poggi C. Diagonal shear behavior of historic walls strengthened with composite reinforced mortar (CRM). Mater Struct 2019;52(6). https://doi.org/10.1617/s11527-019-1414-1.
[5] Scandolo L, Podestà S. The effect of transversal connection in the in-plane response of double-leaf brick masonry walls. In Review, preprint; May 2021. 10.21203/rs.3.rs-488143/v1.
[6] Gattesco N, Rizzi E, Bez A, Dudine A. Study on the effectiveness of a CRM system: in-plane and out-of-plane cyclic tests on masonry piers. Proc Struct Integr 2023;44:2230–7. https://doi.org/10.1016/j.prostr.2023.01.285.
[7] Boem I, Gattesco N. Characterization of textile-reinforced mortar: state of the art and detail-level modeling with a free open-source finite-element code. J Compos Constr 2022;26(5):04022060. https://doi.org/10.1061/(ASCE)CC.1943-5614.0001240.
[8] Boem I. Masonry elements strengthened with TRM: a review of experimental, design and numerical methods. Buildings 2022;12(9):1307. https://doi.org/10.3390/buildings12091307.
[9] Gu J-B, Tao Y, Xin R, Yang Z, Shi Q-X. Seismic performance of multistorey masonry structure with openings repaired with CFRP grid. Adv Civil Eng 2018;2018:1–11. https://doi.org/10.1155/2018/4374876.
[10] Triller P, Tomaževič M, Gams M. Seismic strengthening of clay block masonry buildings with composites: an experimental study of a full scale three-storey building model. Bull Earthq Eng 2019;17(7):4049–80. https://doi.org/10.1007/s10518-019-00609-0.
[11] Lucchini SS, Facconi L, Minelli F, Plizzari G. Cyclic test on a full-scale unreinforced masonry building repaired with steel fiber-reinforced mortar coating. J Struct Eng 2021;147(6). https://doi.org/10.1061/(ASCE)ST.1943-541X.0003020.
[12] Morici M, Gioiella L, Micozzi F, Zona A, Dudine A, Grassia S, et al. Push 'o ver: in situ pushover tests on as built and strengthened existing brickwork constructions. Proc Struct Integr 2023;44:830–7. https://doi.org/10.1016/j.prostr.2023.01.108.
[13] Maddaloni G, Di Ludovico M, Balsamo A, Maddaloni G, Prota A. Dynamic assessment of innovative retrofit techniques for masonry buildings. Compos Part B Eng 2018;147:147–61. https://doi.org/10.1016/j.compositesb.2018.04.038.
[14] De Santis S, de Felice G. Shake table tests on a tuff masonry structure strengthened with composite reinforced mortar. Compos Struct 2021;275:114508. https://doi.org/10.1016/j.compstruct.2021.114508.
[15] Juhásová E, Sofronie R, Bairrão R. Stone masonry in historical buildings — ways to increase their resistance and durability. Eng Struct 2008;30(8):2194–205. https://doi.org/10.1016/j.engstruct.2007.07.008.
[16] Benedetti D, Carydis P, Pezzoli P. Shaking table tests on 24 simple masonry buildings. Earthquake Engng Struct Dyn 1998;27(1):67–90. https://doi.org/10.1002/(SICI)1096-9845(199801)27:1<67::AID-EQE719>3.0.CO;2-K.
[17] Mazzon N, Valluzzi MR, Aoki T, Garbin E. Shaking table tests on two multi-leaf stone masonry buildings. Proc of the 11th Canadian Masonry Symposium, Toronto (Canada), May 31st-June 3rd 2009;vol.
[18] Magenes G, Penna A, Galasco A. A full-scale shaking table test on a two-storey stone masonry building; 2010.
[19] Magenes G, Penna A, Senaldi IE, Rota M, Galasco A. Shaking table test of a strengthened full-scale stone masonry building with flexible diaphragms. Int J Architect Heritage 2014;8(3):349–75. https://doi.org/10.1080/15583058.2013.826299.
[20] Senaldi I, Magenes G, Penna A, Galasco A, Rota M. The effect of stiffened floor and roof diaphragms on the experimental seismic response of a full-scale unreinforced stone masonry building. J Earthq Eng 2014;18(3):407–43. https://doi.org/10.1080/13632469.2013.876946.
[21] Vintzileou E, Mouzakis C, Adami C-E, Karapitta L. Seismic behavior of three-leaf stone masonry buildings before and after interventions: shaking table tests on a two-storey masonry model. Bull Earthq Eng 2015;13(10):3107–33. https://doi.org/10.1007/s10518-015-9746-x.
[22] Guerrini G, Senaldi I, Graziotti F, Magenes G, Beyer K, Penna A. Shake-table test of a strengthened stone masonry building aggregate with flexible diaphragms. Int J Architect Heritage 2019;13(7):1078–97. https://doi.org/10.1080/15583058.2019.1635661.
[23] CONSTRAIN | Italia Slovenia. <https://www.ita-slo.eu/it/constrain> (accessed Mar. 01, 2023).
[24] Gattesco N, Boem I, Rizzi E, Bez A, Gams M, Farič M, Pučnik V, Dudine A. The experimental campaign and numerical simulations of the CONSTRAIN project. Technical report. Standard project co-fincanced by the European Regional Development Fund; 2022.
[25] Langé S. L' eredità romanica: la casa europea in pietra. Jaca Book; 2020.
[26] Roselli G, Mirabile Gattia D, AlShawa O, Cinaglia P, Di Girolami G, Francola C, et al. Mortar analysis of historic buildings damaged by recent earthquakes in Italy. Eur Phys J Plus 2019;134(10):540. https://doi.org/10.1140/epjp/i2019-13024-2.

[27] CEN. EN 1015-11: methods of test for mortar for masonry - Part 11: Determination of flexural and compressive strength of hardened mortar. UNI/CT 021, UNI/CT 021/SC 06; 2019.
[28] CEN. EN 12390-6: testing hardened concrete - Part 6: Tensile splitting strength of test specimens. CEN/TC 104, CEN/TC 104/SC1; 2000.
[29] Gelfi P, Giuriani E, Marini A. Stud shear connection design for composite concrete slab and wood beams. J Struct Eng 2002;128(12):1544–50. https://doi.org/10.1061/(ASCE)0733-9445(2002)128:12(1544).
[30] Lourenço PB, Mendes N, Ramos LF, Oliveira DV. Analysis of masonry structures without box behavior. Int J Architect Herit 2011;5(4–5):369–82. https://doi.org/10.1080/15583058.2010.528824.
[31] Eota. EAD 340392–00-0104: CRM (composite reinforced mortar) systems for strengthening concrete and masonry structures. Euro Org Tech Assess 2018.
[32] ISO. ISO 10406-1: fibre-reinforced polymer (FRP) reinforcement of concrete — Test methods — Part 1: FRP bars and grids. ISO/TC 71/SC 6; 2008.
[33] CEN. EN 12390-3: testing hardened concrete - Part 3: Compressive strength of test specimens. CEN/TC 104; 2001.
[34] CEN. EN 12390-13: testing hardened concrete - Part 13: Determination of secant modulus of elasticity in compression. CEN/TC 104, CEN/TC 104/SC1; 2013.
[35] Boem I, Gattesco N. Cyclic behavior of masonry barrel vaults strengthened through Composite Reinforced Mortar, considering the role of the connection with the abutments. Eng Struct 2021;228:111518. https://doi.org/10.1016/j.engstruct.2020.111518.
[36] NTC. Decreto 17 gennaio 2018: Aggiornamento delle «Norme tecniche per le costruzioni». Italian Ministry of Infrastructure and Transport, Rome, Italy; February 20, 2018.
[37] Brincker R, Zhang L, Andersen P. Modal identification of output-only systems using frequency domain decomposition. Smart Mater Struct Jun 2001;10(3):441–5. https://doi.org/10.1088/0964-1726/10/3/303.
[38] Brincker R., Ventura C., Andersen P. Damping estimation by Frequency Domain Decomposition, Proceedings of IMAC 19: A Conference on Structural Dynamics : februar 5-8, 2001, Hyatt Orlando, Kissimmee, Florida, 2001 (pp. 698-703). Society for Experimental Mechanics.
[39] Oats RC, Dai Q, Head M. Digital image correlation advances in structural evaluation applications: a review. Pract Period Struct Des Constr 2022;27(4). https://doi.org/10.1061/(ASCE)SC.1943-5576.0000725.
[40] Howlader MK, Masia MJ, Griffith MC. Digital image correlation for the analysis of in-plane tested unreinforced masonry walls. Structures 2021;29:427–45. https://doi.org/10.1016/j.istruc.2020.11.051.
[41] Paulson TJ, Abrams DP. Correlation between static and dynamic response of model masonry structures. Earthq Spectra 1990;6(3):573–91. https://doi.org/10.1193/1.1585587.
[42] Tomažević M, Lutman M, Petković L. Seismic behavior of masonry walls: experimental simulation. J Struct Eng 1996;122(9):1040–7. https://doi.org/10.1061/(ASCE)0733-9445(1996)122:9(1040).
[43] Elmenshawi A, Sorour M, Mufti A, Jaeger LG, Shrive N. Damping mechanisms and damping ratios in vibrating unreinforced stone masonry. Eng Struct 2010;32(10):3269–78. https://doi.org/10.1016/j.engstruct.2010.06.016.
[44] Chopra AK. Dynamics of structures: theory and applications to earthquake engineering. 4th ed. Upper Saddle River, N.J: Prentice Hall; 2012.
[45] ATC. FEMA 440. Improvement of nonlinear static seismic analysis procedures, Washington D.C. 2005.
[46] Gattesco N, Boem I. Assessment of the seismic capacity increase of masonry buildings strengthened through the application of GFRM coatings on the walls. IJMRI 2017;2(4):300. https://doi.org/10.1504/IJMRI.2017.087433.
[47] Magenes G. A method for pushover analysis in seismic assessment of masonry buildings. In: Proceedings of the 12th world conference on earthquake engineering, Auckland, New Zealand, 30 January–4 February 2000. New Zealand: Upper Hutt, New Zealand: New Zealand Society for Earthquake Engineering; 2000.
[48] Javed M. Seismic risk assessment of unreinforced brick masonry buildings system of northern Pakistan. PhD Thesis, Department of Civil Engineering, University of Engineering and Technology, Peshawar, Pakistan; 2009.